# An improved index of phase-synchronization for electrophysiological data in the presence of volume-conduction, noise and sample-size bias

Martin Vinck[a,*], Robert Oostenveld[b], Marijn van Wingerden[a], Franscesco Battaglia[a], Cyriel M.A. Pennartz[a]

[a]*Cognitive and Systems Neuroscience Group, SILS Center for Neuroscience, University of Amsterdam, the Netherlands*
[b]*Donders Institute for Brain, Cognition and Behaviour, Radboud University Nijmegen, Nijmegen, The Netherlands*

**Abstract**

Phase-synchronization is a manifestation of interaction between neuronal groups measurable from LFP, EEG or MEG signals, however, volume conduction can cause the coherence and the phase locking value to spuriously increase. It has been shown that the imaginary component of the coherency (ImC) cannot be spuriously increased by volume-conduction of independent sources. Recently, it was proposed that the phase lag index (PLI), which estimates to what extent phase leads and lags between signals from two sensors are nonequiprobable, improves on the ImC. Compared to ImC, PLI has the advantage of being less influenced by phase delays. However, sensitivity to volume-conduction and noise, and capacity to detect changes in phase-synchronization, is hindered by the discontinuity of the PLI, as small perturbations turn phase lags into leads and vice versa. To solve this problem, we introduce a related index, namely the weighted phase lag index (WPLI). Differently from PLI, in WPLI the contribution of observed phase leads and lags is weighted by the magnitude of the imaginary component of the cross-spectrum. We demonstrate two advantages of the WPLI over the PLI, in terms of reduced sensitivity to additional, uncorrelated noise sources and increased statistical power to detect changes in phase-synchronization. Another factor that can affect phase-synchronization indices is sample-size bias. We show that, when directly estimated, both PLI and the magnitude of the ImC have typically positively biased estimators. To solve this problem, we develop an unbiased estimator of the squared PLI, and a debiased estimator of the squared WPLI.

*Keywords:*
Phase relationship; synchronization; oscillation; volume conduction; imaginary; coherence;

## 1. Introduction

Oscillatory neuronal activity has been implied in numerous functions (Buzsáki and Draguhn, 2004; Fries, 2009; Gray et al., 1989; Pesaran et al., 2002; Salinas and Sejnowski, 2001), such as attention, spatial navigation, perceptual binding and memory. Oscillatory activity in different areas can be phase-coupled, i.e., display systematic phase-delays, a phenomenon called phase-synchronization, which has been hypothesized to be an important mechanism for creating a flexible communication structure between brain areas (Engel et al., 2001; Fries, 2005; Varela et al., 2001). In support of this hypothesis, correlations between cognitive functions and long-range phase-synchronization have been demonstrated in many different areas and species, e.g. (Benchenane et al., 2010; Buschman and Miller, 2009; Gregoriou et al., 2009; Pesaran et al., 2008; Roelfsema et al., 1997; Siapas et al., 2005; von Stein et al., 2000; Womelsdorf et al., 2007).

Traditionally, spectral coherence has been used to quantify phase-synchronization for electrophysiological data (EEG and MEG) (Adey et al., 1961; Mitra and Pesaran, 1999; Nunez and Srinivasan, 2006; Walter, 1963). Since coherence merely indicates linear correlation between signals, intermingling phase and amplitude correlations, Lachaux et al. (1999) proposed to use only the relative phase between signals to index phase-synchronization, resulting in an index called the phase locking value (PLV).

However, it is well-known that indexing phase-synchronization can be complicated by four problems: (i) the presence of a common reference, (ii) volume-conduction of source activity, (iii) the presence of noise sources, and (iv) sample-size bias. Volume-conduction of source activity, and, in case of EEG (but not MEG) data, the use of a common reference, can spuriously inflate phase-synchronization indices (Fein et al., 1988; Nolte et al., 2004; Nunez and Srinivasan, 2006; Stam et al., 2007). The problem of volume-conduction is especially large for scalp EEG and MEG data, because of their low spatial resolution. However, it can still be significant when the EEG is measured intracranially (ECoG) or from electrode tips within the tissue (Local Field Potentials - LFPs) if a common reference is used and/or the cross-spectrum is defined over data from spatially close sensors.

To overcome these problems, Nolte et al. (2004) proposed the imaginary component of the coherency (ImC) as a conservative index of phase-synchronization, and showed that volume conduction of uncorrelated sources cannot 'create' a non-zero ImC, based on the conventional assumption that, for typi-

*Corresponding author.
*Email address:* martinvinck@gmail.com (Martin Vinck)

cal EEG and MEG frequencies of interest, the quasi-stationary description of the Maxwell equations holds (Maxwell, 1865; Plonsey and Heppner, 1967; Stinstra and Peters, 1998), implying that the conducted electric activity of a single source affects spatially separate sensors with negligible time delay.

Stam et al. (2007) argued that one disadvantage of the ImC lies in the fact that it can be strongly influenced by the phase of the coherency, so that it is most effective in detecting synchronization with a phase lag corresponding to a quarter cycle, and breaks down if the two sources of interest are in phase or in phase opposition. As a potential improvement on the ImC, Stam et al. (2007) therefore proposed the *phase lag index* (PLI). The PLI estimates, for a particular frequency, to what extent phase leads and lags between signals from two sensors are nonequiprobable, irrespective of the magnitude of the phase leads and lags. In simulations, the PLI performed better than the ImC in detecting true changes in phase-synchronization, and was less sensitive to the addition of volume-conducted noise sources (Stam et al., 2007). Still, PLI's sensitivity to noise and volume conduction may be hindered by the discontinuity in this index as small perturbations turn phase lags into leads and vice versa, a problem that becomes more serious for synchronization effects of small magnitude.

To increase the capacity to detect true changes in phase-synchronization, to reduce the influence of common noise sources (and for EEG data, a common reference) and to reduce the influence of changes in the phase of the coherency, we add a new member to the family of phase-synchronization indices that are based on the imaginary component of the cross-spectrum, namely the *weighted phase lag index* (WPLI). The WPLI extends the PLI in that it weights the contribution of observed phase leads and lags by the magnitude of the imaginary component of the cross-spectrum; in this way it alleviates the discontinuity mentioned above. We will demonstrate two main advantages of the WPLI over the PLI, in terms of their sensitivity to additional, uncorrelated noise sources and their capacity to detect true changes in phase-synchronization.

To bridge the analysis in terms of population parameters to the practical case of data obtained under limited sampling, we will address a final confounding factor that complicates the estimation of phase-synchronization, namely sample-size bias, usually increasing with smaller sample sizes. We will show that the direct PLI estimator (Stam et al., 2007) is positively biased, and that the direct estimator of the ImC's magnitude is typically positively biased, but can be negatively biased as well. To solve this problem, we will introduce an unbiased estimator of the squared PLI and a debiased estimator of the squared WPLI.

The paper is organized as follows. We commence by introducing a conventional linear mixture model (Section 2), and existing indices of phase-synchronization (Section 3). This sets the stage for the definition of the WPLI (Section 4). The comparison of the WPLI with previous statistics will proceed as follows. First, for two correlated sources of interest, we transition from the case of ideal sensors (i.e., neglecting the reference) without volume-conduction to the more realistic case of ideal sensors where the two sources of interest are volume-conducted (Section 5). Second, we continue with a more realistic case where uncorrelated, volume-conducted noise sources have been added (Section 6). Third, we study the effect of changes in the coherency between the activities of two sources of interest (Section 7). After this comparison, we continue with the practical case where population parameters have to be estimated from small sample sizes, (Section 8), and finish our theoretical section by comparing the statistical power of the WPLI and PLI estimators (Section 9). Finally, we apply the proposed techniques to actual LFP data recorded from the rat orbitofrontal cortex (OFC) (Section 10 and 11).

## 2. The linear mixture model

Suppose we observe real-valued signals from two recording sensors, for $N$ trials, and $T$ samples per trial. For every $j$-th trial ($j = 1, \ldots, N$), we receive a $2 \times T$ data matrix $\boldsymbol{S}_j$ where each row of $\boldsymbol{S}_j$ corresponds to data from one of the two sensors. We model the observed data as a linear mixture of $K$ source activities, represented by the $K \times T$ matrix $\boldsymbol{V}_j$. Without loss of generality, we model the observed data in the frequency domain, by using the linearity of the Discrete Fourier Transform (DFT), as

$$\boldsymbol{z}_j(f) = \boldsymbol{A}\boldsymbol{y}_j(f) \tag{1}$$

where $\boldsymbol{z}_j(f) \equiv (z_{1,j}, z_{2,j})^T$ is a vector of complex-valued Fourier spectra, obtained by DFT-ing the respective rows of the data matrix $\boldsymbol{S}_j$; $\boldsymbol{y}_j \equiv (y_{1,j}, \ldots, y_{K,j})^T$ is a vector of complex-valued Fourier spectra whose $k$-th element is obtained by DFT-ing the $k$-th sensor row of $\boldsymbol{V}_j$; and

$$\boldsymbol{A} \equiv \begin{bmatrix} a_{1,1} & \ldots & a_{1,K} \\ a_{2,1} & \ldots & a_{2,K} \end{bmatrix} \tag{2}$$

is a $2 \times K$ matrix of real-valued (not random) coefficients where $a_{1,k}$ and $a_{2,k}$ represent the relative influence of the $k$-th source on the first and the second sensor, respectively. We call the activity of the $k$-th source *volume-conducted* if both $a_{1,k}$ and $a_{2,k}$ are non-zero.

This linear mixture model, which is comparable to the model in Nolte et al. (2004) and Stam et al. (2007), is based on the conventional assumption that the quasi-stationary description of the Maxwell equations holds for the EEG/MEG/LFP frequencies of interest (Plonsey and Heppner, 1967; Stinstra and Peters, 1998); note that this assumption may not be valid for frequencies on the order of kHz (e.g., as with spike-waveforms) (Plonsey and Heppner, 1967; Stinstra and Peters, 1998). The assumption of quasi-stationarity justifies that the elements of $\boldsymbol{A}$ are taken as real-valued and frequency-independent, i.e., do not cause a phase-shift. They can, however, be negative, for example if the two sensors are located in the opposite lobes of a dipole field.

Our goal is to make statements about the statistics of the population from which these data are drawn, i.e., about population parameters. We therefore take the data, in a particular trial, to be the observed outcomes of a vector of random variables,

such that certain outcomes (data) occur with certain probabilities. This gives rise to the linear mixture model in terms of random variables,

$$\boldsymbol{Z} = \boldsymbol{A}\boldsymbol{Y} \tag{3}$$

where $\boldsymbol{Y} \equiv (Y_1, \ldots, Y_K)^T$ is a column vector of $K$ complex-valued random variables whose observed values represent, for a particular frequency, the Fourier spectra of the sources' activities, and $\boldsymbol{Z} \equiv (Z_1, Z_2)^T$ is a column vector of two complex-valued random variables, whose observed values represent, for a particular frequency, the Fourier spectra of the signals observed at the two sensors, respectively. In what follows, we will omit the frequency-dependency of $\boldsymbol{Z}, \boldsymbol{Y}$ and related variables in our notation; it is always implicitly assumed.

Let $X$ be a complex-valued random-variable, to which we will refer as the (non-diagonal part of the) *cross-spectrum*, defined as

$$X \equiv Z_1 Z_2^\star \tag{4}$$

where $Z_2^\star$ is the complex conjugate of $Z_2$. We can write $X$ in exponential form as $X = R\exp(i\Theta)$, where $R$ represents magnitude and $\Theta$ the *relative phase*.

For (linearly) *uncorrelated* source activities, we have $\mathrm{E}\{Y_k Y_l^\star\} = 0$, where $\mathrm{E}\{.\}$ is the expected value operator. On the other hand the condition $\mathrm{E}\{Y_k Y_l^\star\} \neq 0, l \neq k$, implies (linearly) *correlated* source activities.

## 3. Existing indices of phase-synchronization

Before introducing the WPLI and conducting an in-depth comparison of the various statistics, we first provide definitions of conventional indices of phase-synchronization in terms of population parameters (for estimation problems, see Section 8).

The complex-valued *coherency* is defined as

$$C \equiv \frac{\mathrm{E}\{X\}}{\sqrt{\mathrm{E}\{M_1^2\}\,\mathrm{E}\{M_2^2\}}}, \tag{5}$$

where $M_1 \equiv |Z_1|$, and $M_2 \equiv |Z_2|$. The *coherence* is defined as $|C|$, and is always less than or equal to 1.

The phase-locking value (PLV) Lachaux et al. (1999)) is defined as the circular resultant length of the relative phases, i.e.,

$$P \equiv |\,\mathrm{E}\{\exp(i\Theta)\}|\,. \tag{6}$$

The observation $C > 0$ or $P > 0$ is usually taken as evidence for underlying source synchronization.

It has been proposed to discard the real component of the cross-spectrum, based on the following intuitive logic (Nolte et al., 2004; Stam et al., 2007): The volume-conducted activity of a single source to two separate sensors determines, in part, the spectral relationship between signals from these two separate sensors ('self-interaction'). From the assumption of quasi-stationarity, it follows that the cross-spectrum between the volume-conducted activity of a single source at two separate sensors has a 0° (in phase, real component maximally positive) or 180° (orthogonal phase, real component maximally negative) phase (see Section 5), i.e., *only* has a real component. This systematic, 'self-interaction' real component can create a non-zero coherence and PLV. The imaginary component of the cross-spectrum, on the other hand, is zero when the cross-spectrum has a 0° or 180° phase, and maximum when it has a phase of ±90°. That is: for it to be non-zero, it requires the phase-delay between signals to be non-zero. Thus, it is not affected by the 0° or 180° cross-spectral relationship between the volume-conducted activity of a single source at two separate sensors.

More formally, let $\Im\{X\}$ and $\Re\{X\}$ denote the imaginary and the real component of the cross-spectrum, respectively. If all sources are uncorrelated, then $\mathrm{E}\{\Im\{X\}\} = 0$, however, with volume-conduction, we typically have the inequality $\mathrm{E}\{\Re\{X\}\} \neq 0$, corresponding to a spurious 'creation' of a non-zero PLV and coherence (Nolte et al., 2004). To solve this problem, Nolte et al. (2004) proposed the ImC, defined as $\Im\{C\}$, as an index of phase-synchronization, based on the rationale that if all sources are uncorrelated, then the equality $\mathrm{E}\{\Im\{C\}\} = 0$ follows from $\mathrm{E}\{\Im\{X\}\} = 0$ and (5). With restrictions, the sign of the ImC, $\mathrm{sgn}(\Im\{C\})$, indicates whether signals from the first sensor tend to phase lead or lag signals from the second sensor, and the strength of phase-synchronization can be indexed by the magnitude of the ImC, i.e., $|\Im\{C\}|$.

Stam et al. (2007) argued that the ImC can be strongly determined by the phase of the coherency and the normalization by the power spectrum, resulting in decreased sensitivity for detecting changes in phase-synchronization, and increased noise-sensitivity. Therefore, Stam et al. (2007) introduced the PLI, which is defined as

$$\Psi \equiv \left|\mathrm{E}\{\mathrm{sgn}(\Im\{X\})\}\right|, \tag{7}$$

where $\Psi \leq 1$, and the *signed PLI* is defined as $\Psi^s \equiv \mathrm{E}\{\mathrm{sgn}(\Im\{X\})\}$.

## 4. The weighted phase-lag index

As will be argued in more detail below, PLI's sensitivity to noise and volume conduction is hindered by the discontinuity in this measure as small perturbations turn phase lags into leads and vice versa, a problem that becomes more serious for synchronization effects of small magnitude (Section 6). Further, improvement can be made in detecting changes in phase-synchronization (Section 7 and 9). Therefore, we introduce a novel measure of phase-synchronization, called the WPLI, as

$$\Phi \equiv \frac{\left|\mathrm{E}\{\Im\{X\}\}\right|}{\mathrm{E}\{|\Im\{X\}|\}} = \frac{\left|\mathrm{E}\{|\Im\{X\}|\,\mathrm{sgn}(\Im\{X\})\}\right|}{\mathrm{E}\{|\Im\{X\}|\}}. \tag{8}$$

The respective numerators of the WPLI and the magnitude of the ImC are identical, and differ only by the normalization in the denominator. The relationship with the PLI lies in the fact that

the WPLI weights $\mathrm{sgn}(\Im\{X\})$ by $|\Im\{X\}|$. Further note that the inequality $0 \leq \Phi \leq 1$ holds, since the WPLI takes its maximum if $\Pr\{\mathrm{sgn}(\Im\{X\}) = 1\} = 1$ or $\Pr\{\mathrm{sgn}(\Im\{X\}) = -1\} = 1$, where $\Pr\{.\}$ denotes probability, in which case $\left|\mathrm{E}\left\{\left|\Im\{X\}\right| \mathrm{sgn}(\Im\{X\})\right\}\right| = \mathrm{E}\left\{\left|\Im\{X\}\right|\right\}$.

Note that the WPLI and the PLI are based solely on the imaginary component of the cross-spectrum. The ImC, on the other hand, normalizes the imaginary component by the signal amplitudes, i.e., it is not based solely on the imaginary component of the cross-spectrum. Adding uncorrelated noise sources causes signal amplitudes to increase, increasing the normalization term of the ImC, while leaving the nominator of the ImC, $\mathrm{E}\{X\}$, unaltered. The magnitude of the imaginary component of the cross-spectrum captures only part of the signal amplitudes; if it captures only a small portion, then consequently the ImC will be small. This may occur despite the fact that the imaginary component of the cross-spectrum may be very systematically distributed, which would indicate strong phase-synchronization. As argued and shown in simulations by Stam et al. (2007), the normalization of the ImC by signal amplitudes may make it more sensitive to adding uncorrelated noise sources and changes in the phase of the coherency (Section 6 and 7).

## 5. Volume-conducting correlated sources of interest

We start by considering the case where we have no noise sources added and two ideal sensors, i.e., where we have a neutral reference (as would be ideal for LFP/EEG) or no reference (as is the case for MEG); the latter reduction is justified because the problem caused by a common reference is identical to the problem of adding a volume-conducted noise source, since referencing can be described as a linear superposition of the potential of the channel of interest with the negative of the potential of the reference channel.

Suppose that our goal is to index the phase-synchronization between the activities of two spatially separate, correlated sources of interest. In the ideal case, there is no volume-conduction, and each recording sensor would exclusively sample from one of the two sources, such that $\boldsymbol{A} = ((a_{1,1}, 0), (0, a_{2,2}))$. In practice however, the activities of the sources of interest are volume-conducted, i.e., $\boldsymbol{A} = ((a_{1,1}, a_{1,2}), (a_{2,1}, a_{22}))$, where the inequalities $|a_{1,1}| > |a_{2,1}|$ and $|a_{2,2}| > |a_{1,2}|$ follow from the assumption that the $k$-th recording sensor ($k = 1, 2$) is spatially selectively sampling the activity from the $k$-th source.

From (3) and (4), it follows that the cross-spectrum between the activities of the two sources is given by the equality

$$X = \underbrace{a_{1,1}Y_1 a_{2,2}Y_2^\star + a_{1,2}Y_2 a_{2,1}Y_1^\star}_{\text{complex-valued}} + \underbrace{\sum_{k=1}^{2} a_{1,k}Y_k\, a_{2,k}Y_k^\star}_{\text{'self interaction', real-valued}} . \quad (9)$$

Because the last term on the right-hand side of (9), to which we henceforth refer to as the 'self-interaction' term (following the terminology of (Nolte et al., 2004)), is real-valued only, the equality $\Im\{-Y_2Y_1^\star\} = \Im\{Y_1Y_2^\star\}$ holds, and for any two complex-valued variables $c_1$ and $c_2$, the equality $\Im\{c_1 + c_2\} = \Im\{c_1\} + \Im\{c_2\}$ holds, the equalities

$$\Im\{X\} = \left(a_{1,1}a_{2,2} - a_{2,1}a_{1,2}\right)\Im\{Y_1Y_2^\star\} \quad (10)$$

and

$$\mathrm{sgn}\left(\Im\{X\}\right) = \mathrm{sgn}\left(a_{1,1}a_{2,2} - a_{2,1}a_{1,2}\right)\mathrm{sgn}\left(\Im\{Y_1Y_2^\star\}\right). \quad (11)$$

follow.

### 5.1. *Effect of volume-conducting correlated sources of interest on the WPLI*

From (8) and (10), the equation $|xy| = |x|\,|y|$ (for any real-valued $x$ and $y$), and the equation $\mathrm{E}\{cU\} = c\,\mathrm{E}\{U\}$ (for any constant $c$ and random variable $U$), it follows that

$$\begin{aligned}\Phi &= \frac{\left|\mathrm{E}\left\{\left(a_{1,1}a_{2,2} - a_{2,1}a_{1,2}\right)\Im\left\{Y_1Y_2^\star\right\}\right\}\right|}{\mathrm{E}\left\{\left|\left(a_{1,1}a_{2,2} - a_{2,1}a_{1,2}\right)\Im\left\{Y_1Y_2^\star\right\}\right|\right\}} \\ &= \frac{\left|\left(a_{1,1}a_{2,2} - a_{2,1}a_{1,2}\right)\right|\left|\mathrm{E}\left\{\Im\left\{Y_1Y_2^\star\right\}\right\}\right|}{\left|\left(a_{1,1}a_{2,2} - a_{2,1}a_{1,2}\right)\right|\mathrm{E}\left\{\left|\Im\left\{Y_1Y_2^\star\right\}\right|\right\}} \\ &= \frac{\left|\mathrm{E}\left\{\Im\left\{Y_1Y_2^\star\right\}\right\}\right|}{\mathrm{E}\left\{\left|\Im\left\{Y_1Y_2^\star\right\}\right|\right\}} \end{aligned} \quad (12)$$

proving that the WPLI is not affected by volume-conducting correlated sources of interest. Surprisingly, the volume-conduction mixture coefficients from $\boldsymbol{A}$ fall away easily.

### 5.2. *Effect of volume-conducting correlated sources of interest on the PLI*

From 7 and 11, and $\mathrm{E}\{cU\} = c\,\mathrm{E}\{U\}$ for a constant $c$ and random variable $U$, it follows that

$$\begin{aligned}\Psi &= \left|\mathrm{E}\left\{\mathrm{sgn}\left(a_{1,1}a_{2,2} - a_{2,1}a_{1,2}\right)\mathrm{sgn}\left(\Im\{Y_1Y_2^\star\}\right)\right\}\right| \\ &= \left|\mathrm{E}\left\{\mathrm{sgn}\left(\Im\{Y_1Y_2^\star\}\right)\right\}\right| \end{aligned} \quad (13)$$

showing that, like the WPLI, the PLI is not affected by volume-conducting correlated sources of interest. From 11, it follows that the sign of the signed PLI can be affected however.

### 5.3. *Effect of volume-conducting correlated sources of interest on the ImC*

It follows from (3) and (5) that

$$\Im\{C\} = \frac{\mathrm{E}\left\{\left(a_{1,1}a_{2,2} - a_{2,1}a_{1,2}\right)\Im\left\{Y_1Y_2^\star\right\}\right\}}{\sqrt{\mathrm{E}\left\{\left|a_{1,1}Y_1 + a_{1,2}Y_2\right|^2\right\}\mathrm{E}\left\{\left|a_{2,2}Y_2 + a_{2,1}Y_1\right|^2\right\}}}. \quad (14)$$

We conclude from (11) that the *sign* of the ImC can be affected by volume-conducting the correlated sources of interest. However, an increase in volume conduction (i.e., a relative increase in $|a_{2,1}|$ and $|a_{1,2}|$ towards $|a_{1,1}|$ and $|a_{2,2}|$, respectively) can both increase and decrease the ImC, depending on the distribution of the relative phase between $Y_1$ and $Y_2$, as will be demonstrated by the following two examples.

*Example (i):* Suppose that $\boldsymbol{A}$ contains only positive elements, and that, for all observations of $Y_1$ and $Y_2$ that have non-zero probability, $\Re\{Y_1 Y_2^*\} > 0$, i.e. the phase lag between the two sources remains between -90° and +90°. It follows that the denominator in (14) increases as a function of $a_{1,2}$ and $a_{2,1}$, but that the magnitude of the numerator in (14) decreases, so that $|\Im\{C\}|$ decreases as well.

*Example (ii):* Suppose, again, that $\boldsymbol{A}$ contains only positive elements, and $|Y_1 + Y_2| \approx 0$ for all observations of $Y_1$ and $Y_2$ that have non-zero probability. If $a_{1,2}$ and $a_{2,1}$ increase to about 50% of $a_{2,2}$ and $a_{1,1}$, respectively, then, the denominator is multiplied by a factor of about $1/4$, while the numerator is multiplied by a factor of about $1 - 1/2 \cdot 1/2 = 3/4$, causing $|\Im\{C\}|$ to increase by a factor of about 3.

## 6. Addition of uncorrelated, volume-conducted noise sources

Suppose that, in addition to our two sources of interest, we start adding $L-2$ noise sources $(Y_3, \ldots, Y_L)$ that are (i) uncorrelated to each other and (ii) uncorrelated to the two sources of interest $Y_1$ and $Y_2$.

For EEG and LFP recordings, a common reference can be thought of as transitioning from the case of an ideal sensor (with electro-neutral or no reference, as with MEG) to adding a single source to the linear mixture with coefficients $(a_{\text{ref}}, a_{\text{ref}})$. As far as uncorrelated noise sources whose activity is picked up by the reference sensor are concerned, we can subsume the reference problem under this subsection.

Let $X^0$ be the 'true' cross-spectrum before the addition of the noise sources (with an ideal sensor), whose imaginary component is defined as $\Im\{X^0\} \equiv \Im\{(a_{1,1}Y_1 + a_{1,2}Y_2)\,(a_{2,1}Y_1 + a_{2,2}Y_2)^\star\}$. The imaginary component of the resulting cross-spectrum, after addition of the noise sources, is given as

$$\Im\{X\} = \Im\{X^0\} + \Im\{X^\epsilon\}, \tag{15}$$

where

$$\Im\{X^\epsilon\} \equiv \sum_{l=3}^{L}\sum_{k=1}^{K}(a_{1,l}a_{2,k} - a_{2,l}a_{1,k})\,\Im\{Y_l Y_k^\star\} \tag{16}$$

is a real-valued random variable, and $X^\epsilon$ a complex-valued random variable. The equality $\mathrm{E}\{\Im\{X^\epsilon\}\} = 0$, implying $\mathrm{E}\{\Im\{X^0\}\} = \mathrm{E}\{\Im\{X\}\}$, follows from the assumption that the noise sources are all uncorrelated to each other and to the two sources of interest., i.e., $\mathrm{E}\{Y_l Y_k^\star\} = 0$ for $3 \le l \le L$.

Superimposition of uncorrelated, volume-conducted noise sources adds a systematic real-valued 'self-interaction' term to the cross-spectrum (9), which may lead to a strong, spurious increase in the coherence and the PLV. On the other hand, the synchronization measures based on the imaginary part of the cross-spectrum, the ImC, the PLI and the WPLI, are in general decreased by noise addition, or (in the case of PLI) are increased only in some less typical cases, in which the relative phase $\Theta^0$ is not independent from the amplitude $R^0$, and/or the distribution of the relative phase is not symmetric and not unimodal.

### 6.1. Effect of uncorrelated noise on the WPLI

We observe that given the event $|\Im\{X^\epsilon\}| \le |\Im\{X^0\}|$, the conditional expectation of $|\Im\{X^0\} + \Im\{X^\epsilon\}|$ is given by

$$E\left\{\left|\Im\{X^0\} + \Im\{X^\epsilon\}\right| \,\middle|\, \left|\Im\{X^\epsilon\}\right| \le \left|\Im\{X^0\}\right|\right\} = E\left\{\left|\Im\{X^0\}\right|\right\}, \tag{17}$$

and given the event $|\Im\{X^\epsilon\}| > |\Im\{X^0\}|$, the conditional expectation of $|\Im\{X^0\} + \Im\{X^\epsilon\}|$ is given by

$$E\left\{\left|\Im\{X^0\} + \Im\{X^\epsilon\}\right| \,\middle|\, \left|\Im\{X^\epsilon\}\right| > \left|\Im\{X^0\}\right|\right\} \ge E\left\{\left|\Im\{X^0\}\right|\right\}. \tag{18}$$

Combined with the equality $\mathrm{E}\{\Im\{X^0\}\} = \mathrm{E}\{\Im\{X\}\}$ and 8, it follows that the WPLI can not be increased, i.e., only be decreased by adding volume-conducted, uncorrelated noise sources. Further, it is decreased only if the probability of observing the event $|\Im\{X^\epsilon\}| > |\Im\{X^0\}|$ exceeds zero, i.e., if $\Pr\{|\Im\{X^\epsilon\}| > |\Im\{X^0\}|\} > 0$, and it is decreased more if $\Pr\{|\Im\{X^\epsilon\}| > |\Im\{X^0\}|\}$ is larger, i.e., if the probability that the cross-spectrum is rotated across the real axis is larger.

### 6.2. Effect of uncorrelated noise on the ImC

Since $\mathrm{E}\{\Im\{X^0\}\} = \mathrm{E}\{\Im\{X\}\}$, the addition of uncorrelated noise sources leaves the numerator of ImC unaffected, but increases signal power (and thereby the ImC's denominator), so that the magnitude of the ImC overall decreases. As pointed out by (Stam et al., 2007), this may be an explanation for the observation from simulations that the ImC is more distorted by adding uncorrelated, volume-conducted noise sources than the PLI (Stam et al., 2007).

### 6.3. Effect of uncorrelated noise on the PLI

Note that whereas the equality $|\mathrm{E}\{\Im\{X^0\}\}| = |\mathrm{E}\{\Im\{X\}\}|$ holds, the equality $|\mathrm{E}\{\mathrm{sgn}(\Im\{X^0\})\}| = |\mathrm{E}\{\mathrm{sgn}(\Im\{X\})\}|$ in general does not, although, similar to the WPLI, it holds if $\Pr\{|\Im\{X^\epsilon\}| > |\Im\{X^0\}|\} = 0$. Consider the typical (or ideal) case in which the relative phase $\Theta^0$ is distributed according to a unimodal, symmetric circular distribution with a fixed amplitude $R^0$. Without loss of generality we take the circular mean direction of $\Theta^0 \in [0, \pi]$ . Adding uncorrelated noise sources will transform more relative phases with positive sine components into relative phases with negative sine components than vice versa. Thus, the inequality $|\mathrm{E}\{\mathrm{sgn}(\Im\{X\})\}| \le |\mathrm{E}\{\mathrm{sgn}(\Im\{X^0\})\}|$ follows.

However, as was not discussed by Stam et al. (2007), PLI may increase in less typical cases, such as the bimodal one discussed in Section 6.4 (under the heading *Distribution ii*) and in the following example: Suppose that $\Theta^0$ is uniformly distributed on the circle. In addition, suppose that $R^0$ is much larger if $\Im\{X\} \geq 0$ than if $\Im\{X\} < 0$, i.e., that $\Pr\{R^0 = 10, \Im\{X\} \geq 0\} = 1/2$ and $\Pr\{R^0 = 1, \Im\{X\} < 0) = 1/2$. Note that for this distribution, the equality $|\mathrm{E}\{\mathrm{sgn}(\Im\{X^0\})\}| = 0$ holds. When $\mathrm{E}\{|\Im\{X^\epsilon\}|\}$ is relatively small, $X^\epsilon$ will be more likely to cause $\Im\{X\}$ to become positive when $\Im\{X^0\}$ is negative, than to cause $\Im\{X\}$ to become negative when $\Im\{X^0\}$ is positive. Consequently, the inequality $|\mathrm{E}\{\mathrm{sgn}(\Im\{X\})\}| > |\mathrm{E}\{\mathrm{sgn}(\Im\{X^0\})\}|$ follows for this example.

In general, adding uncorrelated noise source may also increase PLI in the more typical case of a unimodal, but asymmetric distribution of relative phases. For the PLI to be nonzero, it is required that the median, i.e., the point that divides a probability distribution in half, of the imaginary component of the cross-spectrum is different from zero. Suppose that the median is zero however, such that the PLI equals zero, but that the mean of the imaginary component exceeds zero, because the imaginary components with a positive sign have a larger magnitude on average (such that the coherence exceeds zero as well). In that case, adding uncorrelated noise sources may rotate more cross-spectra with a negative imaginary component across the real axis than cross-spectra with a positive imaginary component, corresponding to an increase in PLI.

### 6.4. *Comparison of noise-sensitivity of the PLI and WPLI*

The examples above can be understood given that the sign function in the PLI introduces a step-like non-linearity around the real axis, which may amplify noise. If $|\Im\{X^0\}|$ is relatively small, then relatively low-amplitude noise can rotate the cross-spectrum across the real axis, changing the sign of its imaginary component from -1 to +1. Consequently, for small values of $|\Im\{X\}|$ in the presence of noise, we are less confident about the observed phase lead or phase lag. Conversely, if $|\Im\{X\}|$ is large, then we are more confident that the observed phase lead or phase lag corresponds to a 'true' phase lead or phase lag. The problem is alleviated by the weighing procedure introduced with the WPLI: the magnitude of the imaginary component of the cross-spectrum is relatively small when the cross-spectrum is rotated across the real axis, implying more gradual changes to the WPLI when noise sources cause the cross-spectra to rotate across the real axis.

This rationale is illustrated in Figure 1. Shown in Figure 1A are cross-spectra observed over multiple trials before the addition of noise. In Figure 1B, the addition of uncorrelated noise sources causes one of the cross-spectra (indicated in red) to rotate across the real axis. The PLI (Figure 1C) and the WPLI (Figure 1D) can be understood as applying different weights to the sign (indicated by blue and red color) of the imaginary component of the cross-spectrum. When noise rotates a cross-spectrum across the real axis, then, for the PLI, the outcome value for this cross-spectrum changes from +1 to -1, even though the cross-spectrum is very close to the real axis. The WPLI, on the other hand, assigns a small weight to a cross-spectrum undergoing a small rotation across the real axis.

We substantiated this rationale with numerical simulations. The imaginary component of the cross-spectrum was modeled as $\Im\{X\} = \Im\{\exp(i\,\Theta^0)\} + i\,\sigma\epsilon$, where $\Theta^0$ is the relative phase between the two sources of interest, $\epsilon$ is an uniformly distributed random variable on the interval [-1, 1], and $\sigma$ controls the noise amplitude. Here and in the following simulations, because the squared PLI and the squared WPLI can be estimated with a significant reduction in estimator bias (as will be demonstrated further below), we will display the values of these statistics instead of the (unsquared) PLI and the (unsquared) WPLI. We examine two cases. First, a more typical case in which both PLI and WPLI are decreasing functions of noise. Second, a less typical case, in which PLI (but not WPLI) may increase with noise for certain parameter regimes.

*Distribution (i):* The phase $\Theta^0$ was distributed according to the von Mises density function (e.g., Fisher (1993)), defined as

$$P(\theta; \mu, \kappa) \equiv \frac{1}{2\pi I_0(\kappa)} \exp(\kappa \cos(\theta - \mu)). \tag{19}$$

where $I_0(\kappa)$ is defined as the modified Bessel function of order zero, $\mu$ is the circular mean phase, and $\kappa$ the circular dispersion. For all $\kappa \in \{1/9, 3/9, 5/9, 7/9, 1\}$ and $\mu \in \{\pi/8, 2\pi/8, 3\pi/8, \pi/2\}$, we drew $N = 10^7$ observations from the von Mises distribution (samples are always generated following Best and Fisher (1979)). Figure 2A and 2B show that, respectively, the PLI and WPLI are decreasing as a function of noise amplitude $\sigma$, especially for $\mu$ close to the real axis. The main point of Figure 2 is that the addition of noise causes a stronger decrease in the PLI than in the WPLI. Initially, the quotient of the squared WPLI over the squared PLI, i.e., $\Phi^2/\Psi^2$, lies between 1 and 1.7, i.e., the WPLI always exceeds the PLI. For all parameter choices, the ratio converges to values around 6 as we increase the noise amplitude (Figure 2C).

*Distribution (ii):* The relative phase was distributed according to $\Pr\{\Theta^0 = \pi/2\} = 1/2$, and $\Pr\{\Theta^0 = -\pi/100)\} = 1/2$, i.e., there was an equal probability of observing $\Theta^0 = \pi/2$ and $\Theta^0 = -\pi/100$ (these two respective values were arbitrarily chosen, the main point is that $\pi/2$ lies around the imaginary axis and $-\pi/100$ lies closer to, and on the other side of the real axis). We drew $10^8$ observations from this distribution. Figure 3 shows the PLI and the WPLI as a function of noise amplitude $\sigma$. In the regime of relatively small noise amplitudes, the PLI is an increasing function of noise amplitude (Fig 3). If we observe $\Theta^0 = -\pi/100$, then low-amplitude noise is capable of rotating the corresponding cross-spectrum across the real axis, i.e., changing the sign of the imaginary component of the cross-spectrum. Only when the noise amplitude equals the magnitude of the 'true' cross-spectrum, it attains enough 'torque' to rotate the cross-spectrum across the real axis when we observe $\Theta^0 = \pi/2$, causing the PLI to become a decreasing function of noise amplitude. Conversely, in this case as well, the WPLI is a smoothly decreasing function of the noise amplitude (Figure 3) for all values of the noise parameter.

## 7. Detecting changes in the coherency between sources' activities

Having investigated the effect of adding noise and volume-conduction, we will now investigate to what extent the descriptive statistics are affected by changes in (i) the phase and (ii) the magnitude of the coherency (or, the PLV (6)). The influence of components (i) and (ii), which are the typical parameters of interest in neuroscience experiments, are treated separately in this section.

### *7.1. Influence of phase of coherency on WPLI, PLI and ImC*

As pointed out by Stam et al. (2007), a potential disadvantage of the magnitude of the ImC as an index of the strength of phase-synchronization, lies in the fact that its value is not merely determined by the magnitude, but also strongly by the phase of the coherency. First, we will discuss the consequences of changes in the relative phase between the sources of interest in the absence of volume conduction, and we will discuss the effect of volume conduction in the next subsection.

Clearly,

$$|\Im\{C\}| = \left|\frac{\Im\{C\}}{|C|}\right| |C| \,. \tag{20}$$

where $\Im\{C\}/|C|$ equals $\sin(\arg\{C\})$, i.e., the sine of the phase of the coherency. It follows that the dynamic range of the ImC's magnitude (5) is determined directly by the phase of the coherency: for a given $C$, even for maximal coherence $|C| = 1$, ImC's magnitude will be at most $|\Im\{C\}/|C||$. In addition, it follows from (20) that if the phase of the coherency between the activities of the correlated sources rotates, then, given a fixed value of $|C|$, the ImC's magnitude will change accordingly. In contrast, the WPLI and the PLI always range from 0 to 1, independent of the phase of the coherency. Furthermore, phase changes will affect the WPLI and the PLI only to the extent that the distribution of $\mathrm{sgn}(\Im\{X\})$ changes (see Section 7.3).

*Example*. If $\Pr\{\Theta = \pi/2\} = 1$, and $M_1 = M_2 = 1$, then $|C| = 1$, and $|\Im\{C\}| = 1$. Compare this to the case where $\Theta$ is distributed such that $\Pr\{\Theta = \pi/100\} = 1$, implying $|C| = 1$, but $|\Im\{C\}| = \sin(\pi/100)$, falsely indicating that the 'true' interaction is weak. In contrast, the WPLI and the PLI equal 1 for both distributions of $\Theta$.

### *7.2. Influence of the phase of the coherency on the coherence and the PLV*

If volume conduction is not present, then the coherence and the PLV are not distorted by a rotation of the phase of the coherency. However, *with* volume conduction, a real-valued 'self-interaction' term is added to the cross-spectrum (9), and the extent to which this 'self-interaction' term affects the coherence and the PLV is directly modulated by the true phase of the coherency.

We demonstrated the interaction between phase and the 'self-interaction' volume-conduction term (9) with simulations. The cross-spectrum was defined by the equality $X = \exp(i\,\Theta) + I$, where $I$ equaled $1/2$ (Figure 4A) or 1 (Figure 4B), representing the real-valued 'self-interaction' term that arises due to volume conduction. The relative phase $\Theta$ was von Mises distributed. We then computed, for all $\kappa \in \{1/20, 3/20, \ldots, 79/80\}$, the PLV before (open squares) and after adding the volume-conduction term $I$. Simulations were performed with $10^5$ observations.

Figure 4 shows the PLV after addition of the volume-conduction term $I$ as a function of the mean phase $\mu$ of $\Theta$, and the dispersion parameter $\kappa$ (different lines). The effect of the real-valued 'self-interaction' term on the PLV can be both positive and negative, depending on $\mu$ (Figure 4). For a uniform distribution of relative phases in the absence of volume-conduction, the effect of the real-valued 'self-interaction' term on the PLV is always positive. However, if before addition of the volume-conduction term $I$, the PLV is large, then the effect of the 'self-interaction' term $I$ can be strongly negative as well.

The experimental consequence is that, like with ImC, PLI and WPLI, experimentally observed differences in PLV and coherence values cannot, in the presence of volume-conduction, be interpreted only in terms of the consistency of relative phases, i.e., the strength of phase-synchronization, without making assumptions about the stationarity of the phase of the coherency across experimental conditions. Without this assumption, observed differences in PLV and coherence values merely indicate a change in the distribution of relative phase and amplitude, without separating the mean phase parameter from the phase consistency parameter.

### *7.3. Detecting changes in PLV and magnitude of coherence*

We observe three differences between the WPLI and the PLI with respect to detecting phase-synchronization, and changes therein.

(i) Suppose there are two sources of interest, with their cross-spectrum defined by $X = R\exp(i\,\Theta)$. If the coherence exceeds zero (which typically entails a non-zero PLV), and the phase of the coherency does not equal 0 or 180°, then $|\mathrm{E}\{\Im\{X\}\}|$ exceeds zero as well. Thus, the WPLI, as follows from (8), and the magnitude of the ImC will correctly detect that the activities of the sources are phase-synchronized. This does not necessarily hold for the PLI, because a non-uniform distribution of $\mathrm{sgn}(\Im\{X\})$ is not necessarily implied by a non-zero coherence value (e.g., see Figure 3). To be precise, for the PLI to be non-zero, it is required that the median of the imaginary component of the cross-spectrum differs from zero. However, for many probability distributions of the cross-spectrum, e.g., asymmetric distributions, the mean does not coincide with the median of the imaginary component of the cross-spectrum.

(ii) To compare the performance of WPLI and the PLI in detecting changes in phase synchronization, we studied, in simulation, their behavior as a function of the consistency of relative phases (as indexed by the PLV), by generating a sample of $10^7$ observations from a von Mises distribution, for $\mu \in \{0, \pi/40, \ldots, \pi/2\}$ and parametrizing $\kappa$ such that the PLV ranges in 50 equal steps from 0 to 1. Figure 5 shows the squared PLI and squared WPLI as a function of the mean phase $\mu$ and the PLV. Both the WPLI and the PLI are increasing functions

of the PLV, and are increasing functions of $\mu$ (Figure 5). The WPLI has a steeper relationship with the PLV than PLI does when the PLV lies near zero, suggesting better effectiveness in detecting small increases in synchronization. An implication of the larger WPLI values in terms of higher standardized mean values of its estimator will be explored in Section 9.

(iii) Finally, as shown in Section 6, suppose that the cross-spectrum of the two sources of interest changes such that $X' = X + X^\eta$, where $X^\eta$ is a complex-valued noise-variable with $\mathrm{E}\{X^\eta\} = 0$, then the PLI can, incorrectly, indicate an increase in the strength of phase-synchronization, while the WPLI will correctly indicate a decrease.

## 8. The problem of sample-size bias

We will now study another factor that complicates the use of phase-synchronization indices, namely *sample-size bias*, which is a serious problem when, in practice, the population parameters have to be estimated from only a relatively small sample of trials.

### 8.1. Bias of the direct ImC and PLI estimators

The observed data vector $\boldsymbol{x} \equiv (x_1, \ldots, x_N)$ consists of the measured cross-spectra in $N$ trials, where the $j$-th element of $\boldsymbol{x}$ is defined as $x_j \equiv z_{1,j} z^\star_{2,j}$, where the right-hand side terms are defined in (1). Our goal is to estimate population parameters associated with the vector $\boldsymbol{x}$, e.g., the PLI and the WPLI. We therefore take the input data vector $\boldsymbol{x}$ to be the observed outcome of a vector of independent random variables, each distributed identically to $X$, $\boldsymbol{X} \equiv (X_1, \ldots, X_N)$. The $j$-th element of $\boldsymbol{X}$ can be written in exponential form as $X_j = M_{1,j} \exp(i\,\Theta_{1,j}) M_{2,j} \exp(i\,\Theta_{2,j}) = M_{1,j} M_{2,j} \exp(i\,(\Theta_{1,j} - \Theta_{2,j})) = M_{1,j} M_{2,j} \exp(i\,\Theta_j)$.

The *direct ImC estimator* is defined as

$$\Im\{\hat{C}\} \equiv \frac{\sum_{j=1}^N M_{1,j} M_{2,j} \exp(i\,\Theta_j)}{\sqrt{\left(\sum_{j=1}^N M_{1,j}^2\right)\left(\sum_{j=1}^N M_{2,j}^2\right)}}, \tag{21}$$

the *direct signed PLI estimator* as

$$\hat{\Psi}^s \equiv \frac{1}{N} \sum_{j=1}^N \mathrm{sgn}\Big(\Im\{X_j\}\Big), \tag{22}$$

the *direct PLI estimator* as $\hat{\Psi} \equiv |\hat{\Psi}^s|$, and the *direct PLI-square estimator* as $\hat{\Psi}^2$. The direct signed PLI estimator is an unbiased estimator, since

$$\mathrm{E}\{\hat{\Psi}^s\} = \frac{1}{N} \sum_{j=1}^N \mathrm{E}\Big\{\mathrm{sgn}\Big(\Im\{X_j\}\Big)\Big\} = \Psi^s. \tag{23}$$

In contrast, the direct estimator for the PLI, the relevant quantity for assessment of synchronization strength effects, is positively biased. To prove this, consider Jensen's inequality (Rockafellar, 1997), which states that for any convex function $g$ and random variable $U$, the inequality $\mathrm{E}\{g(U)\} \geq g(\mathrm{E}\{U\})$ holds. By applying Jensen's inequality to the direct PLI estimator, with the convex function $g(U) = |U|$ and the random variable $U = \frac{1}{N} \sum_{j=1}^N \mathrm{sgn}(\Im\{X_j\})$, we obtain

$$\begin{aligned} \mathrm{E}\left\{\left| \frac{1}{N} \sum_{j=1}^N \mathrm{sgn}\Big(\Im\{X_j\}\Big) \right|\right\} &\geq \left| \mathrm{E}\left\{ \frac{1}{N} \sum_{j=1}^N \mathrm{sgn}\Big(\Im\{X_j\}\Big) \right\} \right| \\ &= \left| \frac{1}{N} \sum_{j=1}^N \mathrm{E}\Big\{\mathrm{sgn}\Big(\Im\{X_j\}\Big)\Big\} \right| \equiv \Psi \end{aligned} \tag{24}$$

with the strict inequality holding if the probability distribution of $\Im\{X_j\}$ has non zero mass for both positive and negative values.

We performed simulations to investigate the structure of this bias. For all $2 \leq N \leq 200$, we drew $10^6$ samples from a von Mises distribution with $\mu = \pi/4$. Figure 6 shows the expected value of the direct PLI estimator as a function of $N$. The expected value of the direct PLI estimator is positively biased, especially when the PLI is small.

It is often stated that the direct coherence estimator is positively biased, e.g., see (Benignus, 1969; Maris et al., 2007; Vinck et al., 2010b; Womelsdorf et al., 2006). In fact, as above, positive contributions to the estimator bias arise because of the convexity of the absolute value function which applies to the numerator of (5) to obtain the coherence. For many joint probability distributions of $M_1$, $M_2$ and $\Theta$ these positive contributions prevail. However, other contributions to the bias stem from the terms in the denominator of (5), which may render the direct coherence and magnitude of the ImC estimators negatively biased (see Supplemental Material).

### 8.2. An unbiased estimator of the squared PLI

We will now define an unbiased estimator of the squared PLI, simply called the *unbiased PLI-square estimator*, as

$$\hat{\Omega} \equiv \binom{N}{2}^{-1} \sum_{j=1}^{N-1} \sum_{k=(j+1)}^{N} d(X_j, X_k), \tag{25}$$

where for any two complex-valued random variables $U$ and $V$, the function $d$ is defined as

$$d(U, V) \equiv \mathrm{sgn}\left(\Im\{U\}\right) \mathrm{sgn}\left(\Im\{V\}\right), \tag{26}$$

The normalization $(N(N-1))$ equals the number of 2-combinations (of independent trials). As shown in Figure 7, the unbiased PLI-square estimator is defined by (i) computing the imaginary components of the cross-spectra (Figure 7A), (ii) thresholding them to values of +1 and -1 (Figure 7B) and (iii) computing all the pairwise products (Figure 7C).

Let $X^{(1)}$ and $X^{(2)}$ be two independent random variables, identically distributed to $X$. We define the population parameter corresponding to the unbiased PLI-square estimator as

$$\Omega \equiv \mathrm{E}\Big\{d(X^{(1)}, X^{(2)})\Big\}. \tag{27}$$

The equation $\mathrm{E}\left\{\hat{\Omega}\right\} = \Omega$ holds, since

$$\mathrm{E}\left\{\hat{\Omega}\right\} \equiv \mathrm{E}\left\{\binom{N}{2}^{-1} \sum_{j=1}^{N-1} \sum_{k=(j+1)}^{N} d(X_j, X_k)\right\}$$
$$= \binom{N}{2}^{-1} \sum_{j=1}^{N-1} \sum_{k=(j+1)}^{N} \mathrm{E}\left\{d(X_j, X_k)\right\} = \Omega \qquad (28)$$

Observe that $\Omega$ equals the squared PLI: Define $q \equiv \Pr\{\Im\{X\} > 0\}$. It follows that

$$\Omega = \left(q^2 + (1-q)^2\right) - 2q(1-q) = (2q-1)^2 = \Psi^2. \qquad (29)$$

Thus, the expected value of the unbiased PLI-square estimator equals the squared PLI.

This property of unbiasedness can be intuitively understood by observing that the expected value of $d(X_j, X_k)$ is the same for all $N(N-1)$ 2-combinations, implying that the number of 2-combinations we use to compute an average value of $d(X_j, X_k)$ does not affect the expected value of this average.

However, note that $\hat{\Omega}^{1/2}$ is not defined for $\hat{\Omega} < 0$. Thus, the square root of the unbiased PLI-square estimator is unsuited for estimating the *unsquared* PLI. For computational purposes, it is important to note that the squared PLI estimator can be written as a function of the direct PLI-square estimator by

$$\hat{\Omega} = \frac{N\hat{\Psi}^2 - 1}{N-1}. \qquad (30)$$

By using a similar line of argument as in Vinck et al. (2010b) (see also Supplemental Material), it can be shown that variance of the unbiased PLI-square estimator approaches zero asymptotically, i.e., as $N \to \infty$, $\mathrm{Var}\{\hat{\Omega}\} \to 0$, and hence $\hat{\Omega} \to \Omega$. In other words, $\hat{\Omega}$ is a consistent and unbiased estimator of $\Omega$, and therefore of the squared PLI. Whether the mean squared error (MSE) of the unbiased PLI-square estimator is larger than the MSE of the direct PLI-square estimator, depends on the sample size and the PLI value, however, the unbiased PLI-square estimator has, except for extremely small sample sizes, smaller MSE than the direct PLI-square estimator for low PLI values (Supplemental Material, Figure 2).

### 8.3. Definition of debiased estimator of the squared WPLI

We will now define a debiased (i.e., some sample-size bias remains) estimator of the squared WPLI (8), simply called the *debiased WPLI-square estimator*, as

$$\hat{\Omega}^w \equiv \frac{\sum_{j=1}^{N} \sum_{k\neq j} \Im\{X_j\}\Im\{X_k\}}{\sum_{j=1}^{N} \sum_{k\neq j} \left|\Im\{X_j\}\Im\{X_k\}\right|}. \qquad (31)$$

This estimator can be written as a weighted statistic, i.e.,

$$\hat{\Omega}^w = \frac{\sum_{j=1}^{N} \sum_{k=j+1} W_{j,k}\, d(X_j, X_k)}{N(N-1)\bar{W}}, \qquad (32)$$

where the weight $W_{j,k} \equiv |\Im\{X_j\}\Im\{X_k\}|$, $\bar{W}$ is the average weight, called the *weight normalization*, defined as $\bar{W} \equiv \frac{1}{N(N-1)} \sum_{j=1}^{N} \sum_{k=j+1} W_{j,k}$, and the function $d$ is defined in (26). The *normalized weights* are defined by the expression $W_{j,k} \,/\, (N(N-1)\bar{W})$ and sum up to one. If all weights $W_{j,k}$ equal 1, then (32) simplifies to the unbiased PLI-square estimator.

The debiased WPLI-square estimator is computed by (i) computing the imaginary components of the cross-spectra (Figure 7), (ii) computing the average imaginary component of the cross-spectra (Figure 8, top), and (iii) normalizing by the computed average over the magnitudes of the imaginary component of the cross-spectra (Figure 8, bottom).

The corresponding population parameter of the debiased WPLI-square estimator is defined as

$$\Omega^w \equiv \frac{\mathrm{E}\left\{\Im\{X^{(1)}\}\,\Im\{X^{(2)}\}\right\}}{\mathrm{E}\left\{\left|\Im\{X^{(1)}\}\,\Im\{X^{(2)}\}\right|\right\}} \equiv \Phi^2, \qquad (33)$$

where $\Phi$ is defined by (8), and the second step of (33) follows from the property that for any two independent random variables $U_1$ and $U_2$, the expected value operator is multiplicative, i.e., $\mathrm{E}\{U_1 U_2\} = \mathrm{E}\{U_1\}\mathrm{E}\{U_2\}$. Note that, as $N \to \infty$, $\hat{\Omega}^w \to \Omega^w$, i.e., the debiased WPLI-square estimator is a consistent estimator of the squared WPLI.

### 8.4. Bias of the debiased WPLI-square estimator

Similar to the unbiased PLI-square estimator, the estimation procedure described above avoids the contributions to bias coming from the convexity of the function to be estimated, however, it is possible that the estimator is biased. The reason for this is that the expected value of $\hat{\Omega}^w$ cannot be separated into a sum of $N(N-1)$ expected values, because of the division by $\bar{W}$. The bias of $\hat{\Omega}^w$, which we call a 'weighting bias', arises as follows. For all $N(N-1)$ 2-combinations, let the random variable $W$ be identically distributed to $W_{j,k}$, and define the ratio

$$\zeta_{j,k} \equiv \frac{W_{j,k}/E\{W\}}{W_{j,k}/\bar{W}} = \frac{\bar{W}}{E\{W\}}. \qquad (34)$$

Let the observed value of $W_{j,k}$ be defined as $W_{j,k} = w_{j,k}$. Note that $\mathrm{E}\{\bar{W} \mid W_{j,k} = w_{j,k}\} = \frac{1}{N(N-1)}((N(N-1)-1)\,\mathrm{E}\{W\} + W_{j,k})$. The equation

$$\mathrm{E}\{\zeta_{j,k} \mid W_{j,k}\} = 1 + \frac{W_{j,k} - \mathrm{E}\{W\}}{N(N-1)\,\mathrm{E}\{W\}} \qquad (35)$$

follows. If we observe $\zeta_{j,k} > 1$, then the observed value of the ratio $W_{j,k}/\bar{W}$ underestimates the (population parameter) ratio $W_{j,k}/\,\mathrm{E}\{W\}$. If the observed value of $W_{j,k}$ is relative large, i.e., if $w_{j,k} > \mathrm{E}\{W\}$, then the expected value of the weight normalization, i.e., $\mathrm{E}\{\bar{W} \mid W_{j,k} = w_{j,k}\}$, will also be relatively large. As $N \to \infty$, $\zeta_{j,k} \to 1$ for all $N(N-1)$ 2-combinations, retrieving estimator consistency.

If the WPLI exceeds the PLI, then the debiased WPLI-square estimator will be negatively biased for small sample sizes. If, however, the PLI exceeds the WPLI, then the debiased WPLI-square estimator will be positively biased for small sample sizes. The same sort of 'weighting bias' is inherent to the magnitude of the ImC and the coherence (see Supplemental Material).

To further investigate the bias of the debiased WPLI-square estimator we performed simulations, generating $10^6$ samples from the von Mises distributions with $\mu = \pi/4$ (Figure 9A) and $\mu = \pi/8$ (Figure 9B), respectively. We computed the average debiased WPLI-square estimator and unbiased PLI-square estimator value across samples as a function of $N$. The debiased WPLI-square estimator was negatively biased, and converged rapidly to the squared WPLI (Figure 9). For example, for $N > 30$, the remaining negative bias was very small.

## 9. Comparison between the statistical power of the squared PLI and WPLI estimators

To further characterize the sampling distribution of the unbiased PLI-square estimator and the debiased WPLI-square estimator, we determined the ratio of the sample mean over the sample standard deviation, i.e., the standardized mean. The relative phase was von Mises distributed. Figure 10 shows the standardized mean as a function of sample size, for different values of the phase consistency (colors) and the mean phase (subpanels A and B), separate for the PLI (dotted) and WPLI (solid). As demonstrated in Figure 10, the debiased WPLI-square estimator has a larger standardized mean than the unbiased PLI-square estimator does. The implication of this finding is that, for a von Mises distribution of the relative phase, the debiased WPLI-square estimator has larger statistical power than the unbiased PLI-square estimator, i.e., has a higher probability of correctly rejecting the null hypothesis that there is no phase-synchronization.

## 10. Application to experimental LFP data: Methods

To demonstrate the usefulness of the developed phase-synchronization indices, we applied them to actual neuronal data. Methods on the behavioral paradigm and recordings techniques have been described in detail in (van Wingerden et al., 2010a,b; Vinck et al., 2010b). We recorded LFP activity from the rat orbitofrontal cortex (OFC) by using closely separated (<1mm, smallest horizontal separation between electrodes <200$\mu$m, although the exact distance for a specific sensor pair is unknown) electrodes. Rats were performing a two-odor discrimination task. When the rat sampled the 'Go-odor' (S+), a reward (sucrose solution) was delivered when the rat made a sustained poke (1000 ms) at the fluid well (correct go condition). Conversely, when the rat sampled the 'NoGo-odor' (S-), quinine solution (a bitter substance) was delivered when the rat made a sustained response at the fluid well (incorrect go condition). All data analysis was performed in MATLAB, using the Fieldtrip Toolbox (http://www.ru.nl/neuroimaging/fieldtrip/). Analysis of LFP activity was performed for the 2000 ms period preceding the fluid delivery, while the rat was anticipating rewards. This 2000 ms period was divided into the *movement period* (-2000 ms to -1000 ms), in which rats made whole body-movements towards the fluid well, and the *waiting period* (-1000 ms to 0 ms), in which rats maintained a nose-poke in the fluid well and refrained from whole body movements. All computations were performed separately for the *correct go condition*, which was rewarded with sucrose solution, and the *incorrect go condition*, which was negatively reinforced with quinine solution. For every $t \in \{-2000, -1990, \ldots, -10, 0\}$ ms, the LFP segment in the period $[t - 250, t + 250]$ ms was multiplied by a Hann window function and Fast-Fourier-Transformed, with the number of samples equaling $F_s \times 500$ ms, and the sampling frequency $F_s$ equaling 1874. The frequency resolution thus equaled 2 Hz.

The cross-spectrum for all pairs of two separate LFP sensors was then computed. For every time-frequency point, we computed several 'volume conduction insensitive measures', namely the debiased WPLI-square estimator (31), the unbiased PLI-square estimator (25), the direct PLI square $\hat{\Psi}^2$ (22), the (unsquared) magnitude of the ImC (21). For comparison, we also computed an unbiased, 'volume conduction sensitive measure', namely the PPC (Vinck et al., 2010b), whose expected value equals the squared PLV (population parameter). These statistics where then averaged across all the unique LFP sensor pairs that were available within a given session, and subsequently averaged across the 17 available sessions.

## 11. Application to experimental LFP data: Results

As described in van Wingerden et al. (2010b), LFP 'theta'-band (here about 6Hz) power in OFC was higher during the correct go waiting (for sucrose) period than during the incorrect go waiting (for quinine) period.

However, the latter study did not investigate whether (i) the activities of spatially separate OFC populations become more theta-band coherent during the correct go waiting (for sucrose) period than during the incorrect go waiting (for quinine) period and the movement period, and (ii) whether systematic theta phase delays exist between the activities of spatially separate OFC populations during the movement and the waiting period. These questions are difficult to answer by means of standard indices of phase-synchronization, e.g., the PLV, because these may be spuriously increased or decreased by volume conduction.

Volume conduction may cause both cross-talk between the neuronal sources proximal to each electrode (because of the short inter-sensor distance) and the undesired interference from distance sources. In particular, the rat hippocampus generates very strong field potentials in the theta band, and is a major source of volume conduction that affects many distant, cortical areas (Sirota et al., 2008). Volume-conduction of hippocampal activity is especially expected during the movement period, when the rat makes whole-body movements. In addition, volume-conduction coming from local sources and common referencing is expected to cause an elevation of the PLV (for LFP-LFP pairs) at all time-frequency combinations. These volume-conducted related increases in the PLV should not be accompanied by a concurrent increase in the WPLI (and PLI).

Previously, we have shown that, during the waiting period, spiking activity from OFC electrodes is phase-locked, in the

theta frequency-band, to OFC LFPs from different electrodes, suggesting that there may be true phase-synchronization between spatially separate LFPs that occurs at a non-zero phase-delay (van Wingerden et al., 2010b). If so, then we expect an increase in LFP-LFP WPLI (and PLI) values concurrent with an increase in PLV values.

### *11.1. PPC during waiting and movement period*

We first examined a 'volume conduction sensitive measure' of phase-synchronization. We opted for an unbiased statistic, namely the PPC, because the number of trials per session was relative small and imbalanced, with about three times more trials for the correct (session mean ± SEM was 38.12 ± 3.59) than for the incorrect go condition (13.23 ± 1.96).

Figure 11 shows PPC values as a function of time and frequency, for the correct go waiting (11A) and incorrect go waiting (11B) periods separately. A selective increase in theta-band PPC values was observed during the correct go waiting (for sucrose) period (Figure 11). Based on this finding in isolation, one might conclude that this indicates increased theta-band synchronization between underlying sources. However, in addition, an increase in theta-band PPC values was also observed during the movement period (Figure 11C). This made us suspect volume conduction of hippocampal potentials: in fact, theta-band oscillations can be predominantly observed in the hippocampus during active, whole-body movements, which, in the current task, typically occurred during the movement period, but not during the waiting period. Finally, we observed that for all time-frequency combinations, the baseline PPC values exceeded 0.2, even though the PPC is an unbiased statistic.

### *11.2. WPLI, PLI and ImC during waiting and movement period*

Because the PPC is a 'volume-conduction sensitive' measure, it is possible that all of the observed effects can be explained by volume conduction of local (i.e., OFC activity) and distant sources (e.g., the hippocampus). We therefore investigated the time-frequency patterns of the 'volume-conduction insensitive measures', and report the following three findings.

#### *11.2.1. Comparison of WPLI, PLI and PPC*

(i) The respective theta-band values of the debiased WPLI-square estimator (Figure 12, top panel), the unbiased PLI-square estimator (Figure 12, middle panel), and the direct PLI-square estimator (Figure 12, bottom panel), were selectively elevated during the correct go waiting (for sucrose) period (Figure 12), suggesting that, firstly, the corresponding increase in theta-band PPC values reflects true theta-band synchronization between the activities of spatially separate OFC populations, and that, secondly, this increase in theta-band synchronization corresponds to systematic theta phase delays between spatially separate OFC populations. During the correct go waiting (for sucrose) period, the average mean phase delay between signals from two sensors was, at 6 Hz, 16.97°, which corresponds to a mean delay of 7.86 ms.

(ii) The increase in theta-band PPC values during the movement period was not reflected in the respective values of the debiased WPLI-square estimator and the unbiased PLI-square estimator (Figure 12), consistent with our interpretation of it reflecting volume conduction of hippocampal activity.

(iii) The indiscriminate elevation of PPC values above 0.2 for all time-frequency combinations was not observed for the debiased WPLI-square estimator and the unbiased PLI-square estimator (Figure 12), suggesting that this indiscriminate elevation is caused by volume conduction.

#### *11.2.2. Comparison between estimators of the WPLI, PLI and ImC*

A comparison of the WPLI-square, PLI-square and ImC estimators revealed three differences.

(i) As predicted from Figure 5, the unbiased PLI-square estimator theta peak was smaller than the debiased WPLI-square estimator theta peak, i.e., the debiased WPLI-square estimator had a larger dynamic range than the unbiased PLI-square estimator (Figure 12). Correspondingly, the z-scored (i.e., ratio of mean to SEM) debiased WPLI-square estimator theta values (Figure 13, top panels) were about 50% larger than the z-scored unbiased PLI-square estimator values (Figure 13, bottom panels) during the correct go waiting period, as predicted from Figure 10.

Because the debiased WPLI-square is expected to approach the squared WPLI from below when the WPLI exceeds the PLI, the sample-size bias of the debiased WPLI-square estimator may only have lead to an under-estimation of the difference between PLI and WPLI.

(ii) An estimator bias was visible for the direct PLI-square estimator (Figure 12, bottom panels), especially for the incorrect go condition. Note that a small estimator bias (denoted by the non-zero baseline) is also present for the correct go condition. Consequently, the direct PLI-square estimator values that we observed during the movement period (-2000 to -1000 ms) were higher for the incorrect go condition than for the correct go condition. This spurious difference disappeared when we examined the unbiased PLI-square estimator (Figure 12, middle panels).

(iii) We examined the time-frequency representation of the direct estimator of the magnitude of the ImC (Figure 14). We report three differences with the debiased WPLI-square and unbiased PLI-square estimators.

First, we observed that the theta-band values of the direct estimator of the magnitude of the ImC were in generally much lower than the respective theta-band values of the debiased WPLI-square and the unbiased PLI-square estimators (on the order of 5-10 times smaller, considering that the latter statistics estimate squared population parameters). Thus, the debiased WPLI-square estimator and the unbiased PLI-square estimator indicate a greater strength of theta-band synchronization during the correct go waiting period than the direct estimator of the magnitude of the ImC does, a result that is consistent with Stam et al. (2007).

Second, in comparison to the debiased WPLI-square estimator and the unbiased PLI-square estimator, the direct magnitude

of the ImC estimator yielded less contrast between theta-band values for the correct go and the incorrect go waiting period.

Third, in contrast to the debiased WPLI-square estimator and the unbiased PLI-square estimator, the direct estimator for magnitude of the ImC was less precise in rendering the frequency band that increases spectral power for the correct go waiting period. These differences are presumably caused by the ImC's sensitivity to, firstly, changes in the phase of the coherency, secondly, the addition of uncorrelated noise sources, and, thirdly, volume-conducting the correlated sources of interest (i.e., the OFC populations).

## 12. Discussion

We introduced the WPLI, a novel measure of phase-synchronization. Similar to the PLI (Stam et al., 2007), the WPLI estimates to what extent phase leads and lags between signals from two sensors are nonequiprobable. In contrast with the PLI, the WPLI weighs more the contribution of observations based on the magnitude of the imaginary component. WPLI is also tightly related to the ImC, in that they only differ for the normalization. The main advantage of the WPLI above 'volume-conduction sensitive' indices of phase-synchronization is that the latter have a problem with statistical validity, because they intend to index phase-synchronization, but can be spuriously increased by volume-conduction. In addition, we argued that, in comparison to the ImC and PLI, the WPLI has increased sensitivity to detect phase-synchronization and changes therein. For an overview of all of the discussed phase-synchronization indices and their properties, see Table 1.

The problem of indexing phase-synchronization can be formulated as a detection problem. Based on the sensor data, a decision should be made as to whether neuronal sources of interest are phase-synchronized, and whether they are differentially phase-synchronized depending on experimental condition. There are two types of errors that can be made when a decision is taken as to whether the neuronal sources of interest are phase-synchronized or not. (i) Accepting the null hypothesis that there is no phase-synchronization when there is phase-synchronization at the source level (Type II error for detecting phase-synchronization). (ii) Falsely rejecting this null hypothesis (Type I error for detecting phase-synchronization). Similarly, there are two types of errors that can be made when a decision is taken as to whether there are differences in phase-synchronization between neuronal sources of interest as a function of experimental conditions. (i) Falsely accepting the null hypothesis that there are no differences in phase-synchronization between experimental conditions (Type I error for detecting differences in phase-synchronization). (ii) Falsely rejecting this null hypothesis (Type II error for detecting differences in phase-synchronization). We will interpret our results in terms of these four statistical errors.

### *12.1. Comparison of WPLI and PLI*

We demonstrated several advantages of the WPLI over the PLI, which can be formulated in terms of a lower probability of making Type II errors.

(i) In contrast with the PLI, true phase-synchronization (as indexed by the coherence) is, in the absence of volume conduction and noise, and with the phase of the coherency different from $0^\circ$ or $180^\circ$, always detected by the WPLI, corresponding to a lower probability of making Type I errors in detecting true phase-synchronization.

(ii) For a von Mises distribution of the relative phase, adding uncorrelated noise sources entails a stronger decrease in the PLI than in the WPLI, corresponding to a lower probability (for the WPLI) of making Type II errors in (a) detecting phase-synchronization, and in (b) detecting differences in phase-synchronization.

(iii) For the von Mises relative phase distribution, and no noise sources and volume-conduction added, the relationship between the WPLI and the PLV is steeper around zero PLV values, than it is the case for PLI. Correspondingly, we showed that the ratio of the expected debiased WPLI-square estimator value over the debiased WPLI-square estimator sample variance (i.e., the standardized mean) is larger than the ratio of the expected unbiased PLI-square estimator value over the unbiased PLI-square estimator sample variance. This corresponds to a lower probability, for the WPLI, of making Type II errors in (a) detecting phase-synchronization, and in (b) detecting differences in phase-synchronization.

(iv) When the cross-spectrum between the sources of interest changes such that a complex-valued noise-variable is added to the cross-spectrum (reflecting a change in strength of phase-synchronization between their activities), then this can lead to an increase of the PLI, while the WPLI always decreases, corresponding to, firstly, a lower probability (for the WPLI) of making Type II errors in (a) detecting phase-synchronization, and in (b) detecting differences in phase-synchronization.

### *12.2. Comparison of PLI and WPLI with ImC*

Previously, Stam et al. (2007) compared the PLI with the ImC, and showed that, for simulations of the Kuramoto model of coupled oscillators (Kuramoto, 1975), the PLI was less sensitive to the addition of volume-conducted noise sources, and performed better at detecting true changes in phase-synchronization, indicating a lower probability of making both types of Type II Errors.

The ImC has two important downsides when it comes to making Type II errors in detecting phase-synchronization, and Type I and Type II errors in detecting differences in phase-synchronization. Firstly, as already noted by Stam et al. (2007), it can be strongly affected by the phase of the coherency, which can lead to very small ImC values, and a compressed dynamic range of the ImC when the sources of interest are nearly in phase (or in phase opposition). Secondly, the WPLI and the PLI are more noise robust, as they are unchanged unless the noise is strong enough to change the sign of the imaginary part of the cross-spectrum. On the other hand, the magnitude of the ImC is always decreased by adding uncorrelated noise sources.

### *12.3. Volume-conducting correlated sources of interest*

Nolte et al. (2004) and Stam et al. (2007) only modeled the

effect of volume-conducting uncorrelated sources. Expanding on that, we analyzed to what extent volume-conducting two correlated sources of interest distorts the measurement of their true signal relationship. The PLI and the WPLI are not affected, and in the absence of additional noise sources, their true values can be recovered. In contrast, the magnitude of the ImC can either increase or decrease, depending on the phase of the coherency. This is a relevant result for cases where the sources of interest are spatially close, and where a significant proportion of volume conduction comes from the interacting sources of interest themselves.

### *12.4. Comparison of WPLI with coherence and PLV*

The principal limitation of the WPLI (similar to PLI and ImC) is that it is relatively insensitive to true changes in phase-synchronization when the phase of the coherency lies very close to 0 or 180°. In this phase regime, the coherence and the phase locking value will be more sensitive to true changes in phase-synchronization, i.e., have a lower probability of making Type II errors in detecting phase-synchronization. However, they have a much higher probability of making Type I errors, because they can be strongly spuriously increased by volume-conduction. In other words, the coherence and the PLV provide a less valid measure of phase-synchronization. It is important to mention that volume-conduction can also spuriously decrease the coherence and the PLV (see Figure 4). Thus, it can occur that the WPLI exceeds zero while the PLV or the coherence equal zero. For example, this may occur if phase-synchronization occurs at a phase-delay close to 180° (e.g. Gregoriou et al. (2009)), because the use of a common EEG reference creates the same problem as adding a noise source with volume-conduction coefficients that have the same sign, thus adding a systematic positive real component to the cross-spectrum.

It is difficult to make general statements about whether the WPLI has higher or lower probability of making Type I and Type II errors for detecting changes in phase-synchronization as a function of experimental conditions. A priori, the $K$ sources have different degrees of volume-conduction, and variations in the relative activation of the $K$ sources may cause additional variations in the coherence and the PLV, masking true changes in phase-synchronization. Further, both coherence, PLV, and WPLI can be influenced by the phase of the coherency, which can lead to both Type I and Type II errors when it comes to detecting experimental changes in phase-synchronization. Finally, when the changes in phase-synchronization occur at a zero phase-delay, WPLI may be relatively insensitive (leading to Type II errors in detecting changes in true interactions) in comparison to PLV and coherence.

A second limitation of the ImC, the PLI and the WPLI, which also holds for the coherence and the PLV, is that true interactions are not always occurring proximal to the recording sensors of interest. For example, when rodents make whole body movements, high amplitude hippocampal theta-band activity and phase-delayed theta-band synchronization between CA1 and CA3 activity can be observed. Since CA1 and CA3 have different spatial distances to many distant cortical sites (Sirota et al., 2008), theta-band synchronization between nearby cortical sites that occurs at a phase delay different from 0 or 180° may thus reflect true, yet *distant* interactions between CA1 and CA3 (Sirota et al., 2008). This interpretation problem is not solved by constructing a volume-conduction insensitive measure; it can only be addressed by using source reconstruction or current source density analysis.

For EEG data with a spatially dense, controlled arrangement of electrode positions, the problem of a common reference can be addressed by computing local Laplacians (i.e., second derivatives of raw potentials), also known as current-source-density analysis. This approach in essence removes the effect of a common reference (see Nunez and Srinivasan (2006)). In addition, the local Laplacian can act as a spatial filter with improved spatial resolution. A downside of this approach is that the Laplacian may be more noise-sensitive than raw potentials, especially to high spatial frequency noise, and that it emphasizes superficial local sources (for scalp EEG: within a few centimeters), whereas the raw EEG potentials are more sensitive to spatially extended sources (Nunez and Srinivasan, 2006). Furthermore, the Laplacian can not be used for arrays without a spatially dense, controlled arrangement of electrodes (e.g., the example data). Thus, raw EEG potentials and Laplacians offer complementary views on cortical activity.

### *12.5. Sample-size bias problem*

In the second part of our paper, we addressed the problem of estimator bias. We demonstrated that the direct PLI estimator, in contrast with the direct signed PLI estimator, is a positively biased estimator, especially for low values of the PLI.

To solve this 'bias problem', we introduced an unbiased estimator of the squared PLI, called the unbiased PLI-square estimator, using an estimation procedure similar to that described in Vinck et al. (2010b). We emphasize that the unbiased PLI-square estimator is simply an unbiased estimator of an existing index of phase-synchronization, namely the (squared) PLI; it presents nothing new at the population parameter level.

In addition, we developed a pairwise estimator of the squared WPLI, called the debiased WPLI-square estimator, which removes the type of bias that is inherent to the PLI. However, we demonstrated that because the debiased WPLI-square estimator is a weighted statistic, it suffers from an additional source of bias ('weighting bias'), which is caused by the weights determining their own weight normalization. We showed that, as the sample size decreases, the debiased WPLI-square estimator converges to the unbiased PLI-square estimator value, and as it increases, its expected value converges to the squared WPLI. Nevertheless, we believe that this 'weighting bias' is relatively unproblematic, since the expected debiased WPLI-square estimator value converges fairly rapidly to the squared WPLI, because for large sample sizes, the weights hardly impact their own normalization (Figure 9).

On the level of inferential statistics, the effect of the bias of the debiased WPLI-square estimator might be dealt with by means of randomization statistics (Maris and Oostenveld,

2007), or by repeatedly drawing an equal number of trials per experimental condition, similar to the fixed sample size PLV (Vinck et al., 2010a).

### *12.6. Application to OFC data*

In the third part of our paper, we applied the newly developed WPLI to LFP recordings from the OFC of rats engaging in a two-odor discrimination task. Because the LFP sensors were spatially close (< 1mm, up to < 200$\mu$m), we expected that volume conduction from local OFC sources would pose a problem for measuring phase-synchronization. In addition, measures of theta-band synchronization may be spuriously increased by volume conduction of hippocampal activity (Sirota et al., 2008).

We showed that PPC (an estimator of PLV) (Vinck et al., 2010b) was successful at detecting increased theta frequency synchronization in certain behavioral conditions, but also signaled increased theta synchronization during the movement period, likely a result of volume conduction of hippocampal signals(Sirota et al., 2008). Moreover, PPC yielded an elevated baseline value (above 0.2) for all time-frequency points.

Of these three observations, only the first point was confirmed by the analysis of the WPLI. Theta-band WPLI values (as estimated by the debiased WPLI-square estimator) between LFPs were much higher during the waiting (for sucrose) period than during the incorrect go waiting (for quinine) period and the movement period. The increase in theta PPC values during the movement period was not confirmed by the WPLI analysis, supporting the volume conduction interpretation. The indiscriminate increase in PPC values above 0.2 (not seen in the WPLI) for all time-frequency combinations might be explained by the use of a common reference, common noise, and volume conduction within the OFC.

Thus, the analysis methodologies we developed here may be helpful to detect systematic phase leads and lags corresponding to synaptic delays within the local circuit, and communication between different parts of a brain structure. This has important consequences for the analysis of relationship between brain activity and behavior, in the studied example about different brain dynamical regimes induced by reward or lack thereof. In particular, our current results reinforce our previous conclusion that OFC theta-band oscillations during reward anticipation (but not movement) (van Wingerden et al., 2010b) are locally generated, i.e., do not arise because of volume conduction of distant sources.

The measures and estimation procedures described in this paper are made available in the open source FieldTrip toolbox (http://www.ru.nl/neuroimaging/fieldtrip).

## Acknowledgements

MV was supported by European Union Grant FP7 #217148. RO gratefully acknowledges the support of the BrainGain Smart Mix Programme of the Netherlands Ministry of Economic Affairs and the Netherlands Ministry of Education, Culture and Science.

## References

Adey, W., Walter, D., Hendrix, C., 1961. Computer techniques in correlation and spectral analyses of cerebral slow waves during discriminative behavior. Experimental Neurology 3, 501–524.

Benchenane, K., Peyrache, A., Khamassi, M., Tierney, P. L., Gioanni, Y., Battaglia, F. P., Wiener, S. I., Jun 2010. Coherent theta oscillations and reorganization of spike timing in the hippocampal- prefrontal network upon learning. Neuron 66, 921–36.

Benignus, V., 1969. Estimation of the coherence spectrum and its confidence interval using the fast fourier transform. I.E.E.E. Trans. Audio Electroacoust., 145–150.

Best, D., Fisher, N., 1979. Efficient simulation of the von mises distribution. Journal of the Royal Statistical Society. Series C (Applied Statistics).

Buschman, T. J., Miller, E. K., 2009. Serial, covert shifts of attention during visual search are reflected by the frontal eye fields and correlated with population oscillations. Neuron 63, 386–396.

Buzsáki, G., Draguhn, A., 2004. Neuronal oscillations in cortical networks. Science 304, 1926–1929.

Engel, A. K., Fries, P., Singer, W., Oct 2001. Dynamic predictions: oscillations and synchrony in top-down processing. Nat. Rev. Neurosci. 2, 704–716.

Fein, G., Raz, J., Brown, F., Merrin, E., 1988. Common reference coherence data are confounded by power and phase effects. Electroencephalography and Clinical Neurophysiology 69 (6), 581–584.

Fisher, N., 1993. Statistical analysis of circular data. Cambridge University Press.

Fries, P., 2005. A mechanism for cognitive dynamics: neuronal communication through neuronal coherence. Trends Cogn. Sci. 9, 474–480.

Fries, P., 2009. Neuronal gamma-band synchronization as a fundamental process in cortical computation. Annu. Rev. Neurosci. 32, 209–224.

Gray, C. M., König, P., Engel, A. K., Singer, W., 1989. Oscillatory responses in cat visual cortex exhibit inter-columnar synchronization which reflects global stimulus properties. Nature 338, 334–337.

Gregoriou, G. G., Gotts, S. J., Zhou, H., Desimone, R., 2009. High-frequency, long-range coupling between prefrontal and visual cortex during attention. Science 324, 1207–1210.

Kuramoto, Y., 1975. Self-entrainment of a population of coupled non-linear oscillators. In: International symposium on mathematical problems in theoretical physics. Springer, pp. 420–422.

Lachaux, J. P., Rodriguez, E., Martinerie, J., Varela, F. J., 1999. Measuring phase synchrony in brain signals. Hum Brain Mapp 8, 194–208.

Maris, E., Oostenveld, R., 2007. Nonparametric statistical testing of EEG-and MEG-data. Journal of Neuroscience Methods 164, 177–190.

Maris, E., Schoffelen, J.-M., Fries, P., 2007. Nonparametric statistical testing of coherence differences. J Neurosci Methods 163, 161–75.

Maxwell, J., 1865. A dynamical theory of the electromagnetic field. Philosophical Transactions of the Royal Society of London 155, 459–512.

Mitra, P. P., Pesaran, B., Feb 1999. Analysis of dynamic brain imaging data. Biophys. J. 76, 691–708.

Nolte, G., Bai, O., Wheaton, L., Mari, Z., Vorbach, S., Hallett, M., 2004. Identifying true brain interaction from EEG data using the imaginary part of coherency. Clin Neurophysiol 115, 2292–2307.

Nunez, P. L., Srinivasan, R., 2006. Electric fields of the brain: the neurophysics of EEG. Oxford University Press.

Pesaran, B., Nelson, M. J., Andersen, R. A., 2008. Free choice activates a decision circuit between frontal and parietal cortex. Nature 453, 406–409.

Pesaran, B., Pezaris, J. S., Sahani, M., Mitra, P. P., Andersen, R. A., 2002. Temporal structure in neuronal activity during working memory in macaque parietal cortex. Nat. Neurosci. 5, 805–811.

Plonsey, R., Heppner, D., 1967. Considerations of quasi-stationarity in electrophysiological systems. Bulletin of Mathematical Biology 29, 657–664.

Rockafellar, R., 1997. Convex analysis. Princeton Univ Pr.

Roelfsema, P. R., Engel, A. K., König, P., Singer, W., 1997. Visuomotor integration is associated with zero time-lag synchronization among cortical areas. Nature 385, 157–161.

Salinas, E., Sejnowski, T. J., 2001. Correlated neuronal activity and the flow of neural information. Nat Rev Neurosci 2, 539–50.

Siapas, A. G., Lubenov, E. V., Wilson, M. A., 2005. Prefrontal phase locking to hippocampal theta oscillations. Neuron 46, 141–151.

Sirota, A., Montgomery, S., Fujisawa, S., Isomura, Y., Zugaro, M., Buzsáki, G., 2008. Entrainment of neocortical neurons and gamma oscillations by the hippocampal theta rhythm. Neuron 60, 683–697.

Stam, C. J., Nolte, G., Daffertshofer, A., 2007. Phase lag index: assessment of functional connectivity from multi channel eeg and meg with diminished bias from common sources. Human brain mapping 28, 1178–93.

Stinstra, J., Peters, M., 1998. The volume conductor may act as a temporal filter on the ECG and EEG. Medical and Biological Engineering and Computing 36, 711–716.

van Wingerden, M., Vinck, M., Lankelma, J., Pennartz, C., 2010a. Learning-associated gamma-band phase-locking of action-outcome selective neurons in orbitofrontal cortex. J. Neurosci. 30, 10025–10038.

van Wingerden, M., Vinck, M., Lankelma, J., Pennartz, C., 2010b. Theta-band Phase-locking of Orbitofrontal Neurons during Reward Expectancy. J. Neurosci. 30, 7078–7087.

Varela, F., Lachaux, J. P., Rodriguez, E., Martinerie, J., 2001. The brainweb: phase synchronization and large-scale integration. Nat. Rev. Neurosci. 2, 229–239.

Vinck, M., Lima, B., Womelsdorf, T., Oostenveld, R., Singer, W., Neuenschwander, S., Fries, P., 2010a. Gamma-phase shifting in awake monkey visual cortex. J. Neurosci. 30, 1250–1257.

Vinck, M., van Wingerden, M., Womelsdorf, T., Fries, P., Pennartz, C. M. A., 2010b. The pairwise phase consistency: A bias-free measure of rhythmic neuronal synchronization. NeuroImage.

von Stein, A., Chiang, C., König, P., 2000. Top-down processing mediated by interareal synchronization. Proc. Natl. Acad. Sci. U.S.A. 97, 14748–14753.

Walter, D., 1963. Spectral analysis for electroencephalograms: mathematical determination of neurophysiological relationships from records of limited duration. Experimental Neurology 8, 155–181.

Womelsdorf, T., Fries, P., Mitra, P. P., Desimone, R., Feb 2006. Gamma-band synchronization in visual cortex predicts speed of change detection. Nature 439, 733–736.

Womelsdorf, T., Schoffelen, J. M., Oostenveld, R., Singer, W., Desimone, R., Engel, A. K., Fries, P., 2007. Modulation of neuronal interactions through neuronal synchronization. Science 316, 1609–1612.

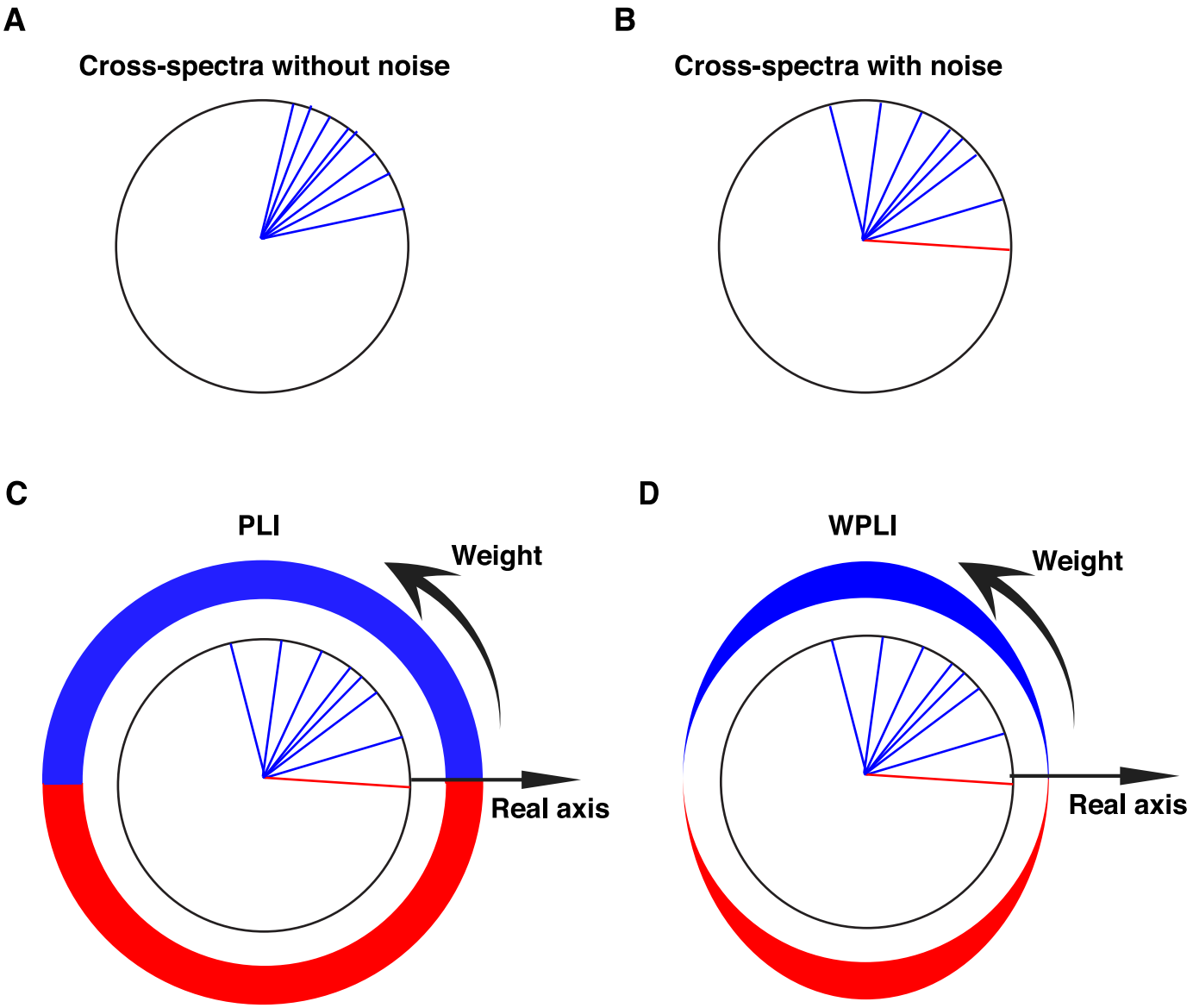


Figure 1: Illustration of the WPLI and the PLI. (A) Cross-spectra without noise. (B) Cross-spectra with noise, causing one of the cross-spectra to rotate across the real axis. (C) PLI weights all cross-spectra equally, and assigns a value of +1 (blue; phase lead) or -1 (red; phase lag) depending on which side of the real axis a cross-spectrum lies. (D) WPLI weights cross-spectra according to the magnitude of the imaginary component of the cross-spectrum. Cross-spectra around the real axis contribute to a lesser extent than cross-spectra around the imaginary axis.

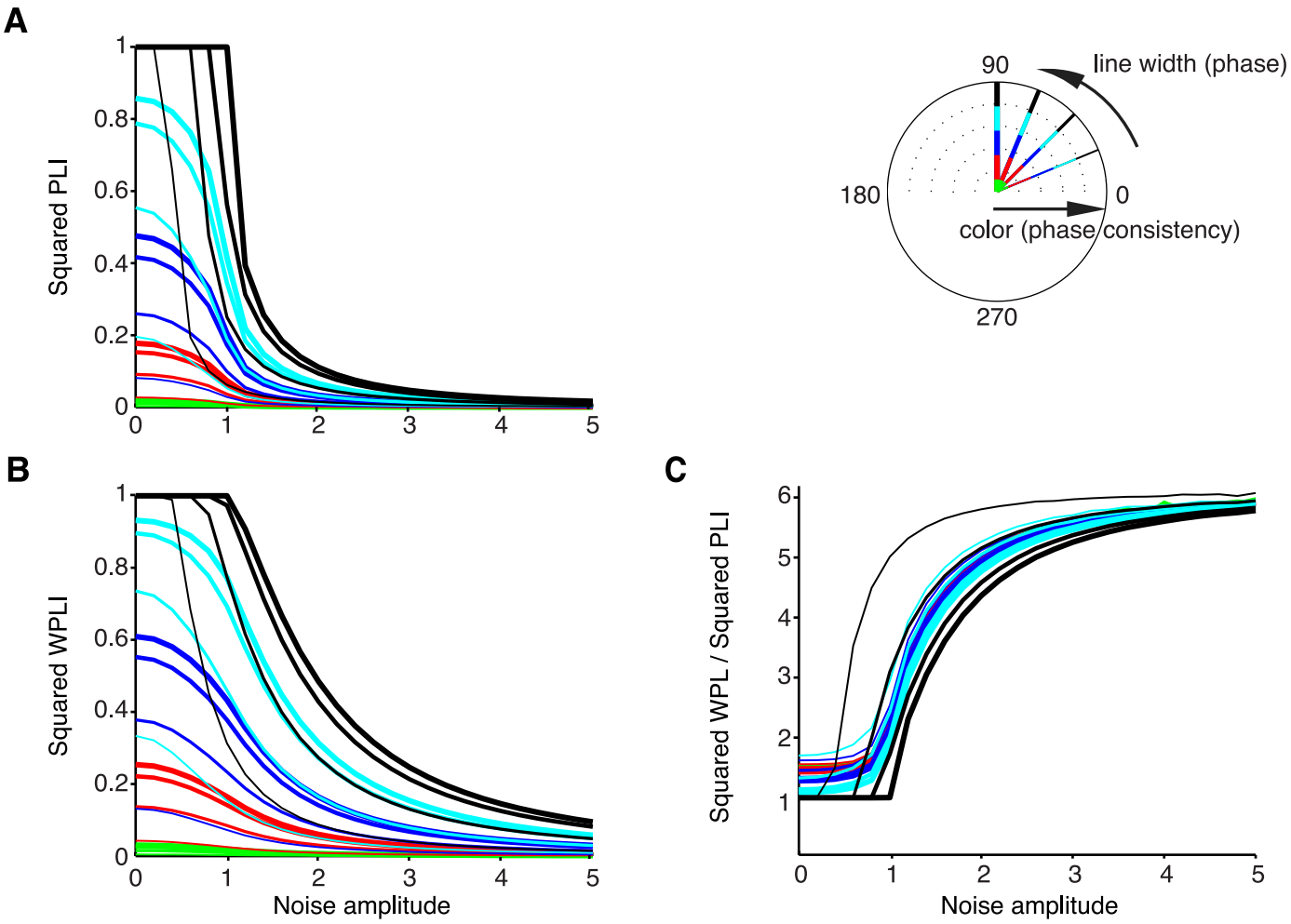


Figure 2: Influence of noise on the PLI and the WPLI for a von Mises distribution. (A) The squared PLI, $\Psi^2$, as a function of the noise amplitude $\sigma$. (B) Correspondence of line width and line color with $\mu$ and the PLV values, respectively. (C) Same as in (A), but now for the squared WPLI, $\Phi^2$. (D) Same as in (A), but now shown the ratio $\Phi^2/\Psi^2$. Values > 1 indicate larger squared WPLI values.

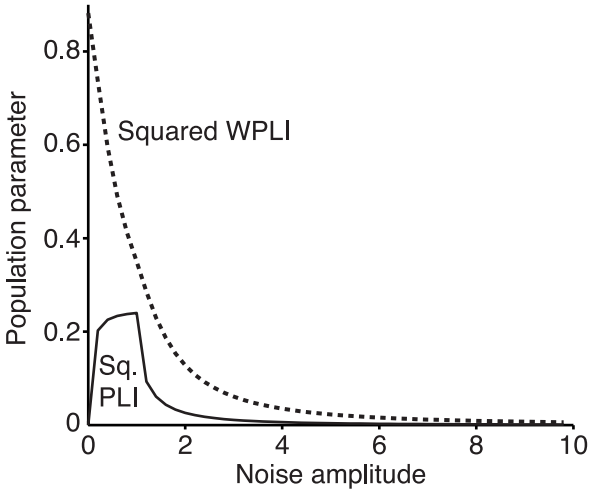


Figure 3: Dependence of the PLI and the WPLI on the addition of uncorrelated noise sources, for a bimodal distribution of the relative phase. X-axis: values of noise amplitude $\sigma$. Y-axis: population parameter after addition of noise.

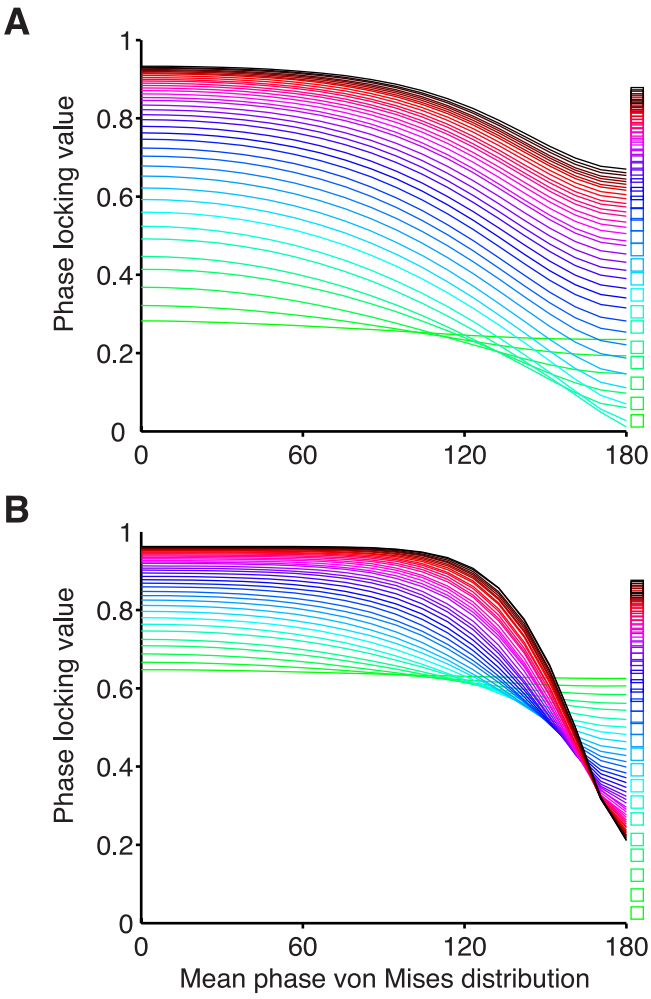


Figure 4: Relationship between the circular mean phase and the PLV. (A) The PLV, after addition of a real-valued 'self-interaction' volume-conduction term ($V = \frac{1}{2}$), as a function of true mean phase of the underlying von Mises distribution. Open squared indicate PLV values without addition of 'self-interaction' term. Green-to-black color-scaling indicates increasing values of the PLV. (B) Same as in (A), but now with real-valued 'self-interaction' term $V = 1$.

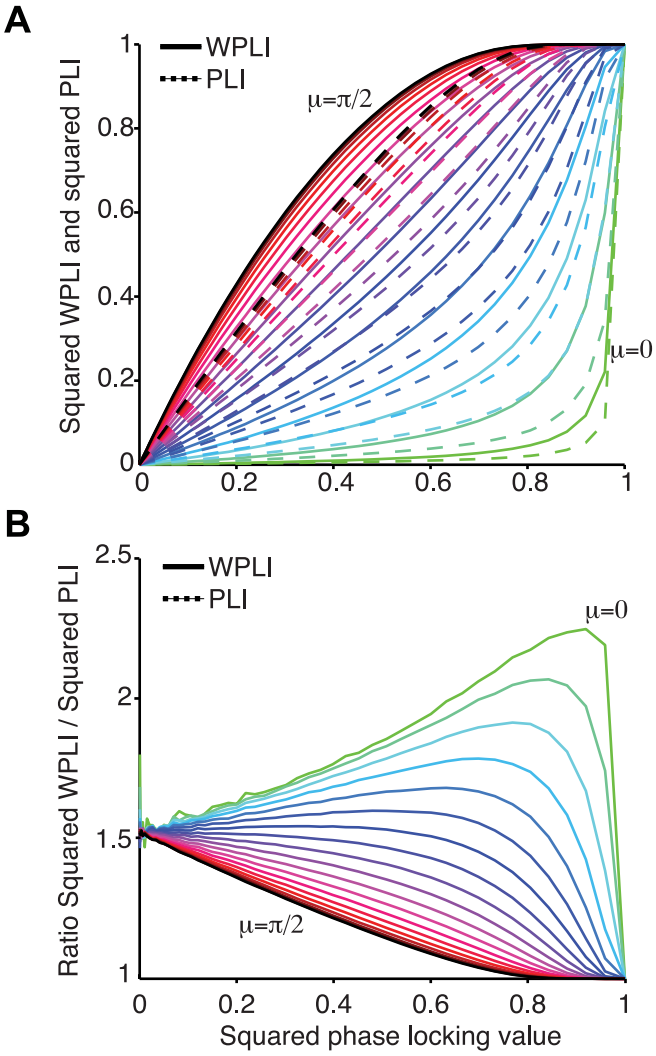


Figure 5: Relationship of the squared WPLI and the squared PLI on the one hand to the squared PLV on the other hand, for a von Mises distribution. (A) X-axis: the squared PLV. Solid lines: the squared WPLI. Dashed lines: the squared PLI. Green-to-black color scaling indicates increasing values of $\mu \in \{0, \pi/40, \ldots, \pi/2\}$. (B) Same as (A), but shown the quotient of the squared WPLI over the squared PLI, i.e., $\Phi^2/\Psi^2$. Values > 1 indicate a larger squared WPLI.

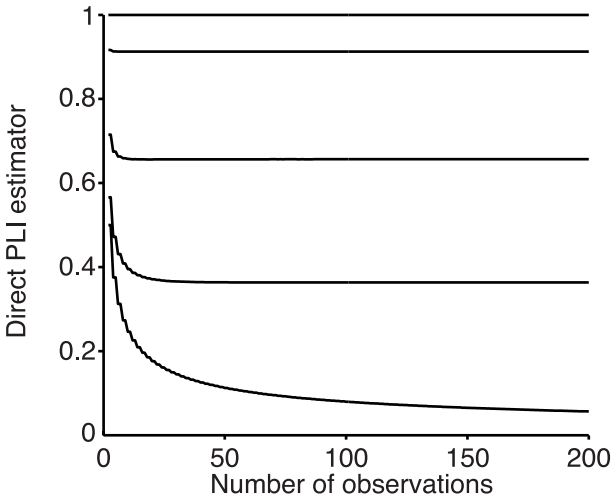


Figure 6: Bias of the direct PLI estimator, for a von Mises distribution. The expected value of the direct PLI estimator for a different number of observations. Lines from bottom to top represent increasing values of the PLV ($\{0, 4/10, 7/10, 1\}$).

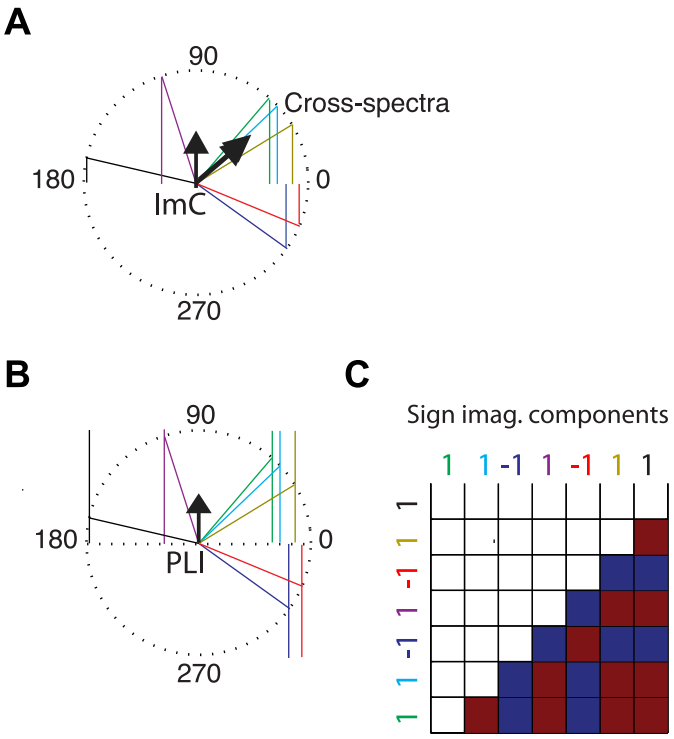


Figure 7: Illustration of the ImC, the PLI and the unbiased PLI-square estimator. (A) Each line originating from the center of the circle represents a cross-spectrum, with the magnitude fixed. The coherency and its projection on the imaginary axis (ImC) are shown as black arrows. Vertical lines originating from the endpoints of the cross-spectra represent their corresponding imaginary components. (B) Same as in (A), but the vertical lines originating from the endpoints of the cross-spectra now represent the signs of their corresponding imaginary components. The PLI is defined as the magnitude of the expected sign value, and depicted as a black arrow. (C) Unbiased PLI-square estimator is defined as the average of all pairwise products of signs. Pairs with identical observations are excluded (diagonal). Red squares indicate equal signs, blue squares indicate unequal signs. Order of 1's and -1's is irrelevant.

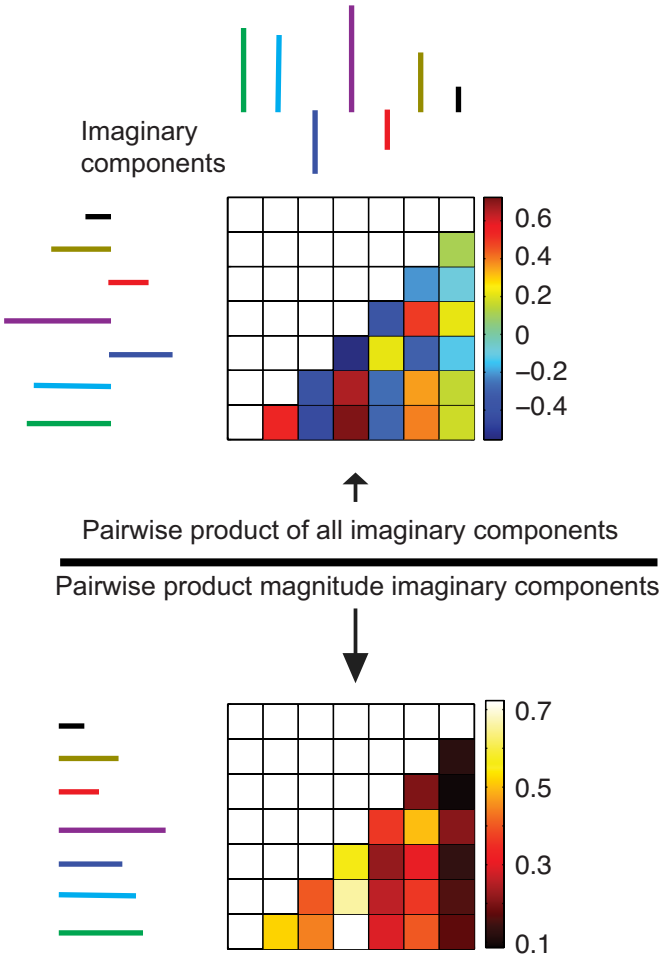


Figure 8: Graphical explanation of debiased WPLI-square estimator. Top: The debiased WPLI-square estimator's numerator is defined as the sum of all pairwise products of imaginary components, that correspond to the imaginary components in Figure 7. Bottom: The denominator of the debiased WPLI-square estimator is defined as the sum of all pairwise products of the magnitudes of the imaginary components.

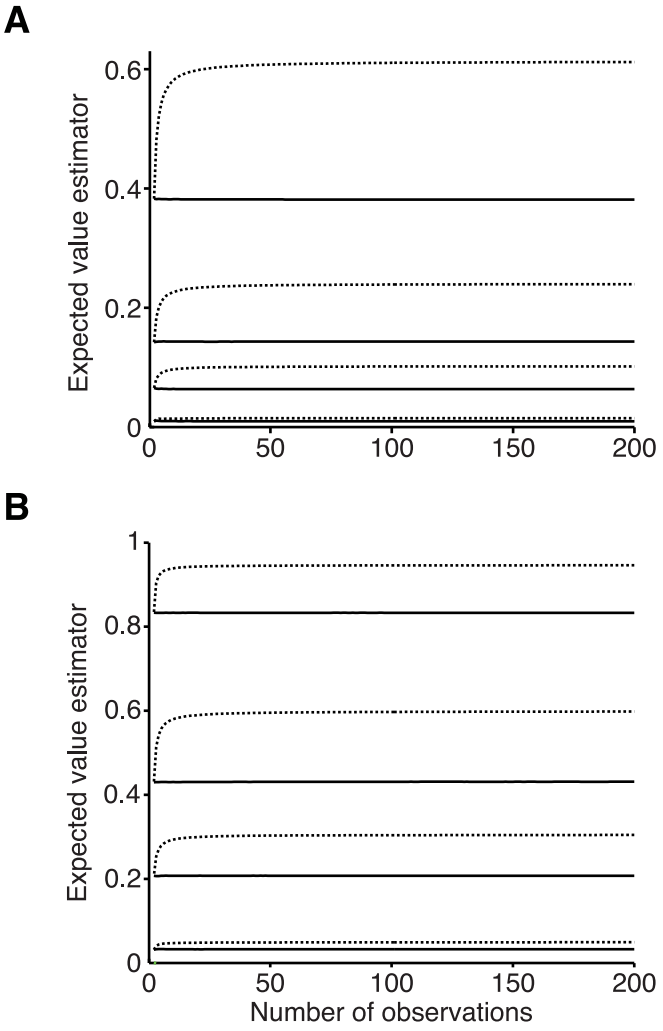


Figure 9: Bias of the debiased WPLI-square estimator and the unbiased PLI-square estimator. (A) Expected value of debiased WPLI-square estimator (dotted lines) and unbiased PLI-square estimator (solid lines) as a function of sample size $N$. Samples were drawn $10^6$ times from a von Mises distribution with $\mu = \pi/16$. Lines from bottom to top correspond to values of PLV $\{2/10, 5/10, 7/10, 9/10\}$. (B) Same as in (A), but now for $\mu = \pi/8$.

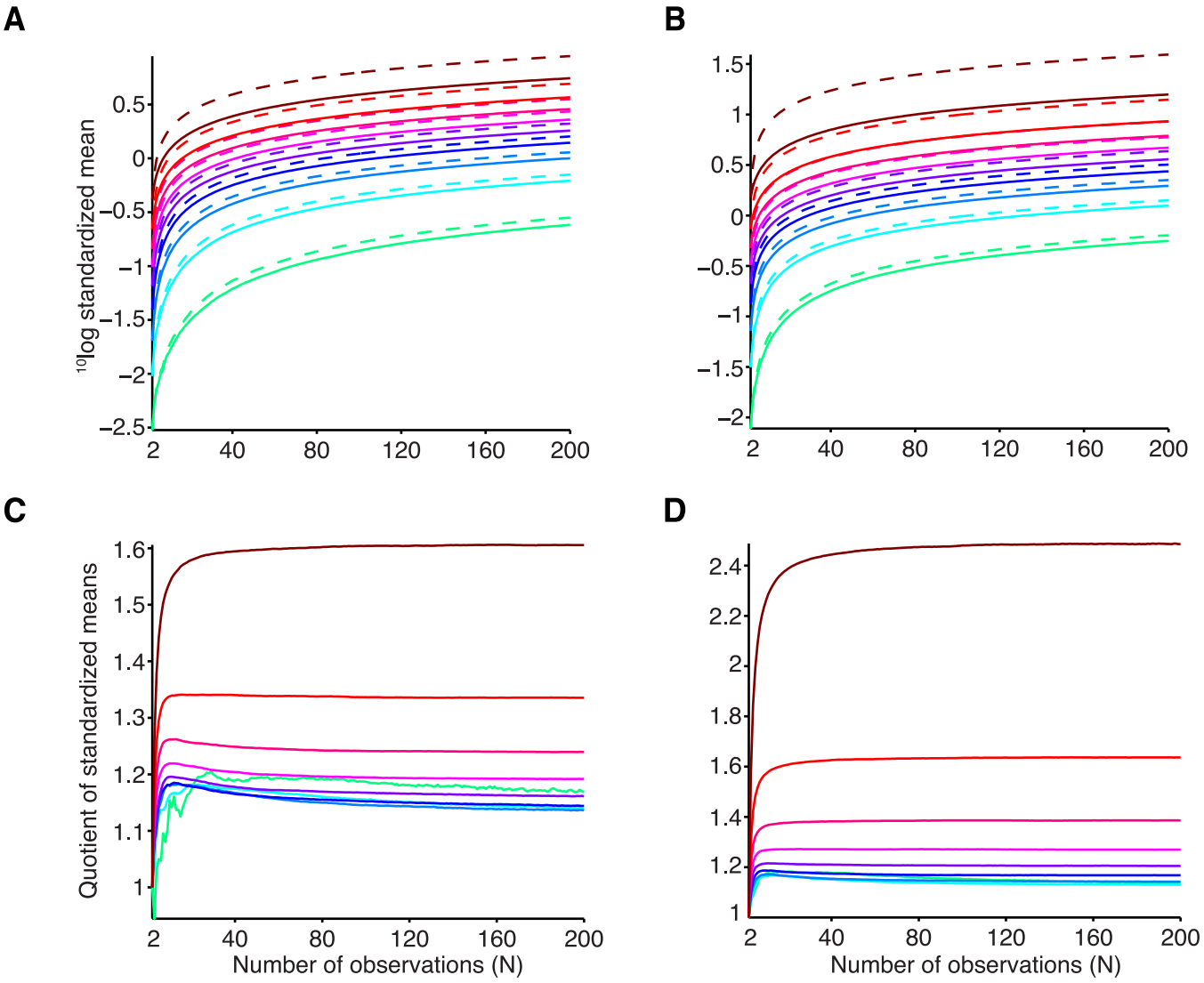


Figure 10: Quotient of sample mean over sample standard deviation compared between unbiased PLI-square estimator and debiased WPLI-square estimator. (A) $^{10}$ log transformed quotient of sample mean over sample standard deviation (standardized mean) as function of $N$ for debiased WPLI-square estimator (dotted) and unbiased PLI-square estimator (solid). Phases were von Mises distributed with $\mu = \pi/8$. Green-to-purple color-scaling indicates increasing values of PLV $\{0.1, 0.2 \ldots, 0.9\}$. (B) Same as in (B), but now $\mu = \pi/4$. (C) $^{10}$ log transformed quotient of debiased WPLI-square estimator standardized mean over unbiased PLI-square estimator standardized mean, for $\mu = \pi/8$. Values $> 1$ indicate larger standardized mean for debiased WPLI-square estimator. (D) Same as in (C), but now $\mu = \pi/4$.

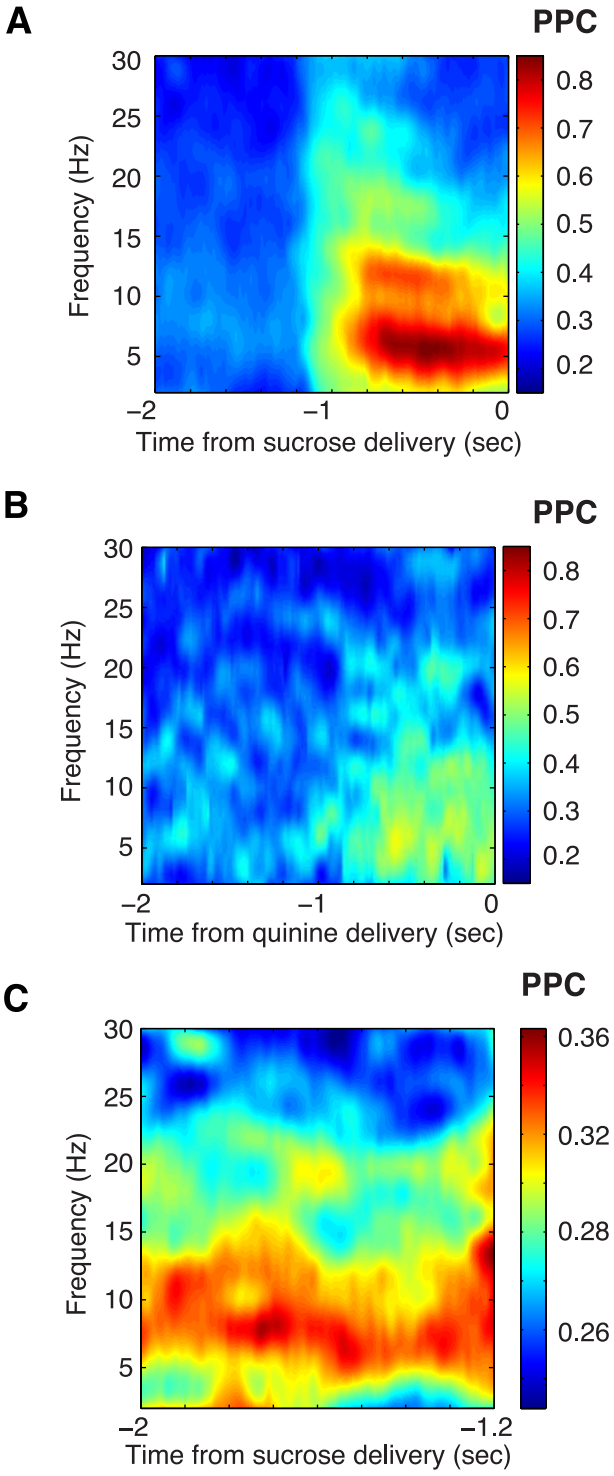


Figure 11: PPC compared between correct go and incorrect go condition. (A) Average PPC as a function of time and frequency during the correct go movement and waiting (for sucrose) period. (B) Same as (A), but now during the incorrect go movement waiting (for quinine) period. (C) Average PPC as a function of time and frequency, separate for the correct go movement period.

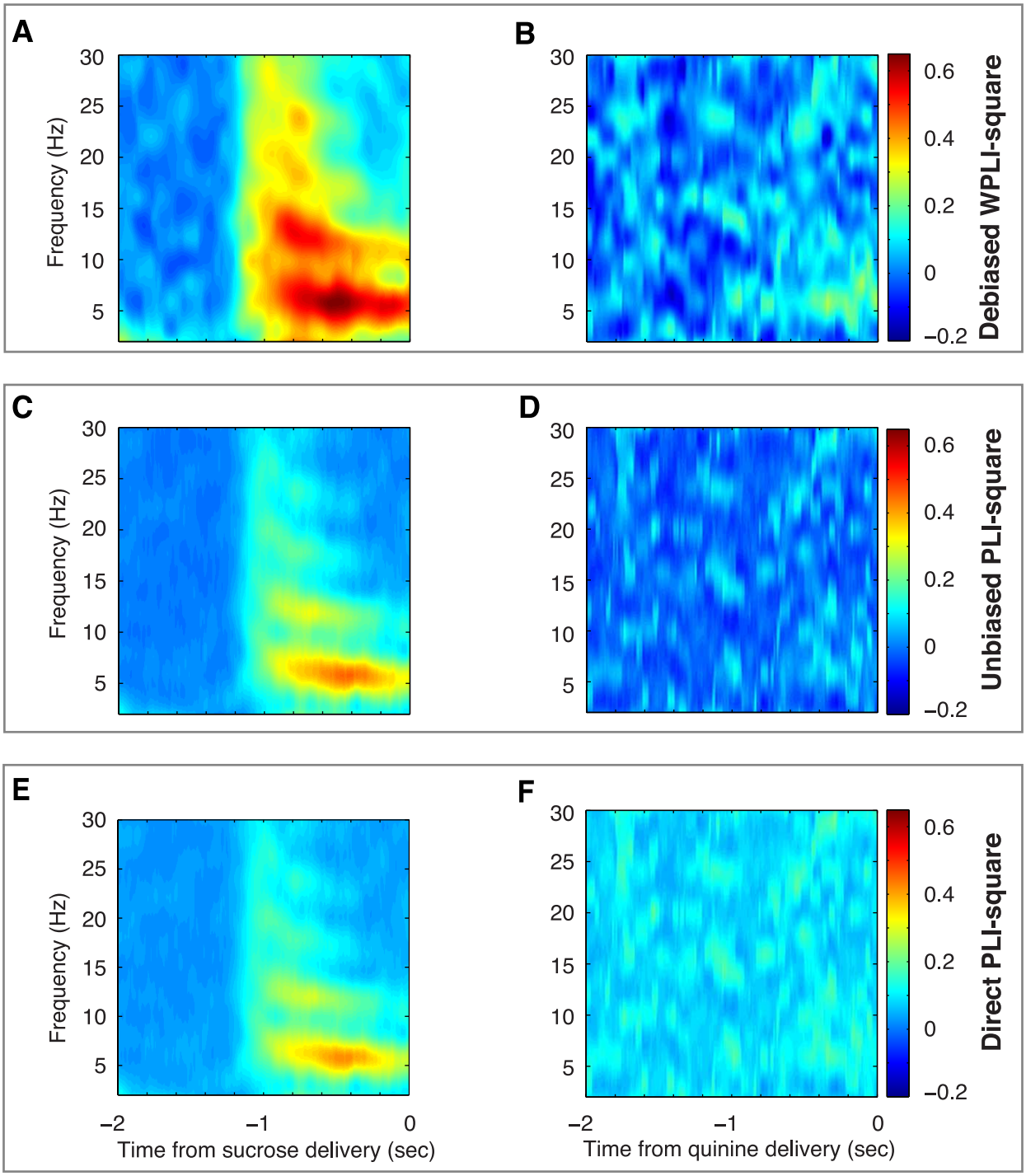


Figure 12: Comparison of debiased WPLI-square estimator, unbiased PLI-square estimator, and direct PLI-square between correct go and incorrect go conditions. All figures have same color scaling to enhance comparability. (A) Average debiased WPLI-square estimator as function of time and frequency during the correct go waiting (for sucrose) period. (B) Average debiased WPLI-square estimator as function of time and frequency during the incorrect go waiting (for quinine) period. (C) Average unbiased PLI-square estimator as function of time and frequency during the correct go waiting (for sucrose) period. (D) Average unbiased PLI-square estimator as function of time and frequency during the incorrect go waiting (for quinine) period. (E) Average direct PLI-square as a function of time and frequency during the correct go waiting (for sucrose) period. (F) Average direct PLI-square as a function of time and frequency during the incorrect go waiting (for quinine) period. Notice the non-zero baseline value in comparison to (D)

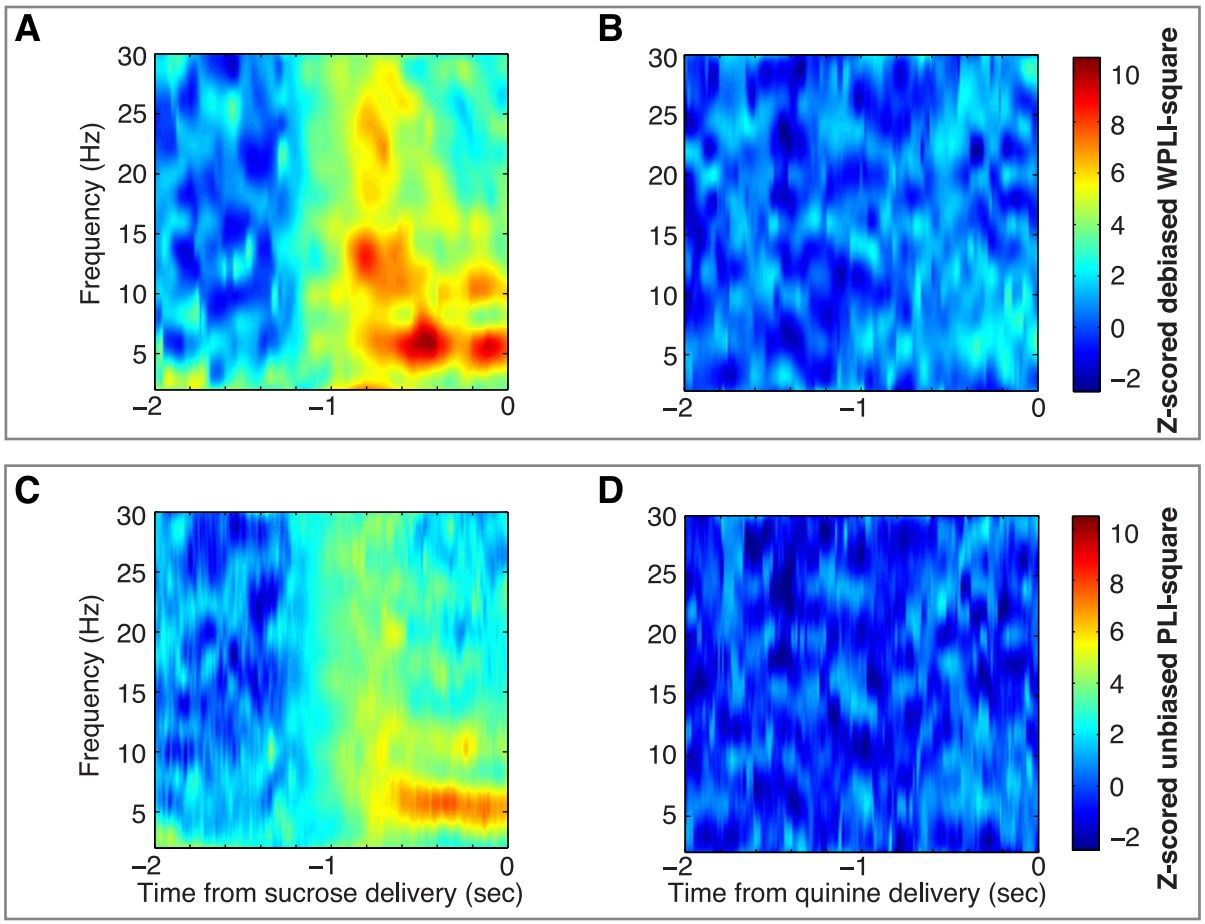


Figure 13: Comparison of z-scored debiased WPLI-square estimator and z-scored unbiased PLI-square estimator. All figures have same color scaling to enhance comparability. (A) Average z-score standardized debiased WPLI-square estimator as function of time and frequency during the correct go waiting (for sucrose) period. (B) Average z-score standardized debiased WPLI-square estimator as function of time and frequency during the incorrect go waiting (for quinine) period. (C) Average z-score standardized unbiased PLI-square estimator as function of time and frequency during the correct go waiting (for sucrose) period. (D) Average z-score standardized unbiased PLI-square estimator as function of time and frequency during the incorrect go waiting (for quinine) period.

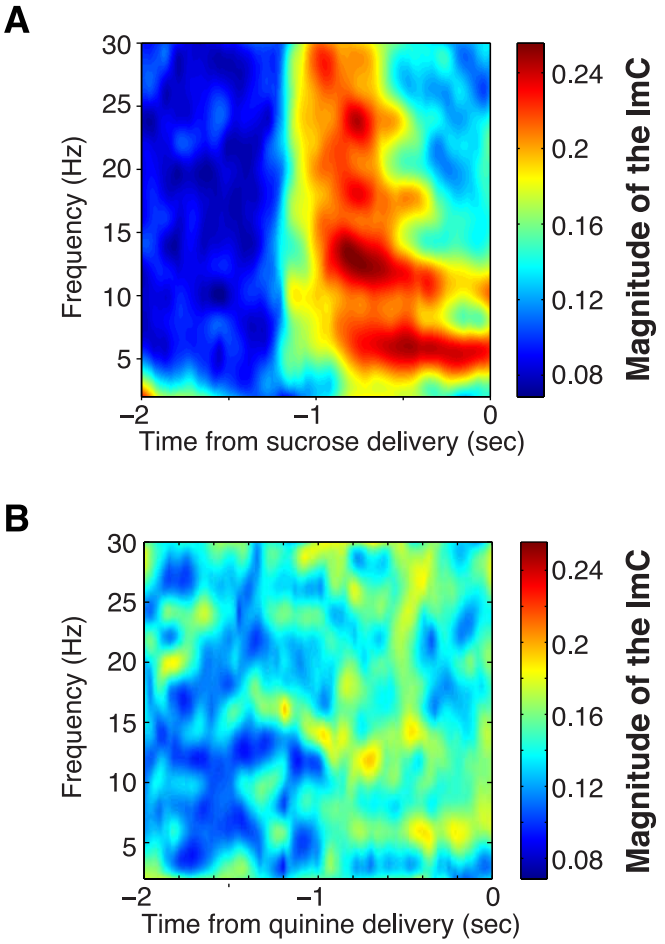


Figure 14: Direct magnitude of the ImC estimator compared between correct go and incorrect go condition. (A) Average direct magnitude of the ImC estimator as a function of time and frequency during the correct go waiting (for sucrose) period. (B) Same as (A), but now during the incorrect go waiting (for quinine) period.

| | Coherence and PLV | ImC (Nolte et al., 2004) | PLI (Stam et al., 2007) | WPLI |
|---|---|---|---|---|
| Construction index (Section 3 and 4). | Uses imaginary and real part equally. | Expected value of imaginary component cross-spectrum, normalized by expected value of signals' power. | Consistency of sign of imaginary component cross-spectrum. | Expected value of imaginary component cross-spectrum, normalization by expected value of magnitude imaginary component cross-spectrum. |
| Effect of volume-conduction correlated sources of interest (Section 5). | Strong increase or decrease, depending on phase of coherency and sign volume-conduction coefficients. | Increase or decrease, depending on phase coherency and volume-conduction coefficients. | Unaffected. | Unaffected. |
| Effect of adding volume-conducted, uncorrelated noise sources (Section 6). | Strong increase or decrease, depending on phase of coherency and volume-conduction coefficients. | Always decreases, because signal amplitudes always increase. | Depending on distribution relative phase, increase (e.g., for some bimodal or asymmetric distributions) or decrease (e.g. for symmetric, unimodal distributions). | Decrease, insofar sign of imaginary component cross-spectrum changes. Less noise-sensitive than PLI. |
| Effect of change in phase of coherency between sources of interest (Section 7.1). | Decrease or increase, depending on volume-conduction coefficients. | Strong increase or decrease possible, range of statistic depends on phase coherency (see also Stam et al. (2007)). | Range statistic is always [0,1], PLI only changes if distribution of sign imaginary component of cross-spectrum is affected. | Range statistic is always [0,1], WPLI only changes if distribution of sign imaginary component of cross-spectrum is affected. |
| Detecting phase-synchronization. | Strong tendency to generate false positives, false positives rate cannot be controlled. | Reduced sensitivity in detection vs. PLI. (Stam et al., 2007). False positives rate controlled. | Even without added noise, PLI may fail to detect phase-synchronization for bimodal/asymmetric relative phase distributions. However, false positives rate controlled. | Even without added noise: Steeper relationship with true phase-consistency (e.g., as measured by PLV) than PLI, always detects non-zero coherence, WPLI estimator has higher z-score than PLI estimator. |

Table 1: Summary of performance and behavior of different phase-synchronization indices.

*Negative bias of the coherency*

Since the coherence is a weighted statistic, in the sense that it weights $\exp(i\Theta)$ by the amplitude $R$, it can also be negatively biased for some ranges of the sample size. This type of 'weighting bias' is, in the context of the WPLI's bias, discussed in detail. In short, the negative bias can arise because the weights in the coherence's numerator, i.e., $M_{1j}M_{2j}$, determine their own weight normalization, i.e., the coherence's denominator. The weight normalization is, on expectation, overestimated for large observed values of $M_{1j}$ and $M_{2j}$. If the coherence exceeds the PLV, then the coherence can be negatively biased for some intervals of the sample size $N$. *Example.* Suppose that, for any $A \geq 0$, $\Pr\{\Theta = \frac{1}{2}\pi, R = A\} = \frac{1}{2}$, and $\Pr\{\Theta = \frac{1}{2}\pi, R = 1\} = -\frac{1}{2}$. If $A \neq 1$, then the coherence exceeds the PLV. Supplementary Figure 1 shows that, for this distribution, the direct coherence estimator can approach the coherence from below. Since for this distribution, $\Re\{C\} = 0$, it follows that the direct ImC's magnitude estimator approaches the ImC's magnitude from below as well.

*Variance and consistency of the unbiased PLI-square estimator*

Having examined the first central moment of the unbiased PLI-square estimator, we will now examine its second central moment. The 2-combinations over which it is defined are not statistically independent. This does not affect the expected unbiased PLI-square estimator value, but it does affects its variance, which is given by the equality $\mathrm{Var}\left\{\hat{\Omega}\right\} = \mathrm{E}\{\hat{\Omega}^2\} - \Omega^2$. The first term on the right-hand side of this equation can be expanded as

$$\mathrm{E}\{\hat{\Omega}^2\} = \mathrm{E}\left\{\binom{N}{2}^{-2}\left(\sum_{j=1}^{N}\sum_{k=j+1} d(X_j, X_k)\right)^2\right\}. \tag{1}$$

We can decompose $\mathrm{E}\{\hat{\Omega}^2\}$ in three terms: The product of the ''sign agreement' $d$ for 2-combinations that are identical, the product of the 'sign agreement' for 2-combinations that are independent and the product for 2-combinations in which there is one shared observation, such that the total number of 2-combinations of 2-combinations (for $N > 2$) equals

$$\binom{N}{2} + \binom{N}{2}\frac{(N-2)(N-3)}{2} + \binom{N}{2}(2N-4), \tag{2}$$

which equals $\binom{N}{2}^2$. By expanding (1), the variance of the unbiased PLI-square estimator equals

$$\begin{aligned}\mathrm{Var}\{\hat{\Omega}\} = {} & \frac{2}{N(N-1)}\mathrm{E}\{d(X^{(1)}, X^{(2)})^2\} \\ & + \frac{6-4N}{N(N-1)}\Omega^2 + \frac{4N-8}{N(N-1)}\mathrm{E}\{d(X^{(1)}, X^{(2)})\, d(X^{(1)}, X^{(3)})\},\end{aligned} \tag{3}$$

where $X^{(3)}$ is a random variable identically distributed to and independent from $X$. It follows from (3) that the variance of the iPPC approaches zero asymptotically, i.e., as $N \to \infty$, $\mathrm{Var}\left\{\hat{\Omega}\right\} \to 0$, and hence $\hat{\Omega} \to \infty$. In other words, $\hat{\Omega}$ is a consistent and unbiased estimator of $\Omega$.

*Comparison of mean squared error between direct squared PLI and unbiased PLI-square estimator*

Removing the bias from a statistical estimator may lead to an increase in the estimator's variance. An estimator's *mean squared error* (MSE), which is defined as the sum of the bias and the variance, captures both quantities at once. We directly compared the MSE of the unbiased PLI-square estimator to the MSE of the direct PLI-square by generating $10^6$ samples from a discrete Bernoulli probability distribution, defined by the probabilities $q \equiv \Pr\{\mathfrak{I}\{X\} > 0\}$ and $1 - q = \Pr\{\mathfrak{I}\{X\} < 0\}$, with $q \in \{0, 1/60, \ldots, 1/2\}$. For values of $q$ close to $\frac{1}{2}$, the MSE of the unbiased PLI-square estimator compares favorably to the MSE of the direct PLI-square for a wide range of sample sizes ($N > 10 - 20$), while it is only slightly larger for small values of $q$. For very small sample sizes, especially $N < 5$, the MSE of the direct PLI-square compares favorably to the MSE of the unbiased PLI-square estimator (Supplementary Figure 2), for both small and large PLI. Thus, whether the MSE of the unbiased PLI-square estimator compares favorably to the MSE of the direct PLI-square depends on $N$ and the PLI.

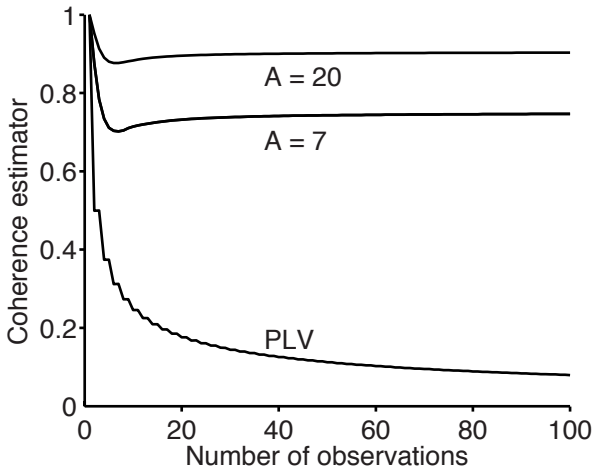


Figure 1: Expected value of coherence estimator $\hat{C}$ as a function of sample size $N$. Cross-spectra $X = R\exp(i\Theta)$ were distributed according to $\Pr\{\Theta = \frac{1}{2}\pi, R = A\} = \frac{1}{2}$, and $\Pr\{\Theta = -\frac{1}{2}\pi, R = 1\} = \frac{1}{2}$. Each line corresponds to a different value of $A$ ($A \in \{1, 7, 20\}$).

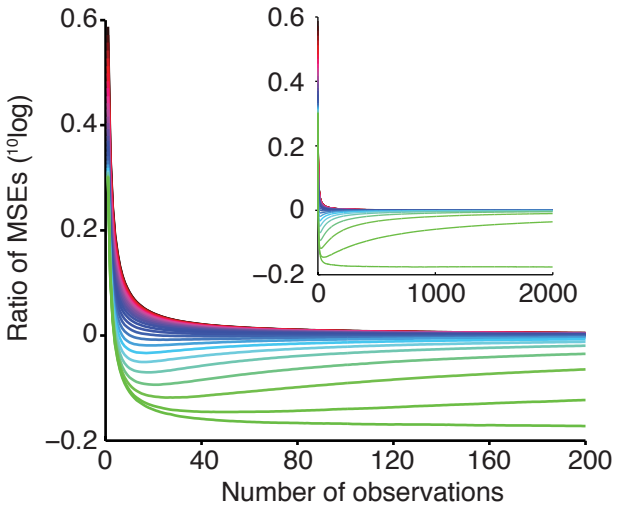


Figure 2: The $^{10}$ log transformed quotient of the MSE of the unbiased PLI-square estimator, over the MSE of the direct PLI-square, i.e., $^{10}\log(\mathrm{E}\{(\hat{\Omega} - \Omega)^2\}/\,\mathrm{E}\{(\hat{\Psi}^2 - \Psi^2)^2\}$. Increasing values of the PLI ($\{0, 1/30, \ldots, 1\}$) are indicated by green-to-black color scaling. Values of zero indicate to equal MSE. Values $> 0$ indicate larger MSE for the unbiased PLI-square estimator. Inset: MSE quotient for larger samples.